Naa12 rescues embryonic lethality in *Naa10*-Deficient Mice in the amino-terminal acetylation pathway

Hyae Yon Kweon[1¶], Mi-Ni Lee[1,#a¶*], Max Dörfel[2], Seungwoon Seo[1], Leah Gottlieb[3,4], Thomas Papazyan[2], Nina McTiernan[5], Rasmus Ree[5], Andrew Garcia[6], Michael Flory[7], Jonathan Crain[2], Alison Sebold[2], Scott Lyons[2], Ahmed Ismail[2], Elaine Marchi[8], Seong-keun Sonn[1], Se-Jin Jeong[9], Sejin Jeon[1], Shinyeong Ju[10], Simon J. Conway[17], TaeSoo Kim[1], Hyun-Seok Kim[1], Cheolju Lee[10,11], Tae-Young Roh[12], Thomas Arnesen[5,13,14], Ronen Marmorstein[3,4,15], Gholson J. Lyon[2,6,16*], and Goo Taeg Oh[1*]

[1]Department of Life Science and College of Natural Sciences, Ewha Womans University, Seoul, Republic of Korea
[2]Stanley Institute for Cognitive Genomics, Cold Spring Harbor Laboratory, Woodbury, New York, United States of America
[3]Department of Chemistry, University of Pennsylvania, Philadelphia, United States of America
[4]Abramson Family Cancer Research Institute, Perelman School of Medicine, University of Pennsylvania, Philadelphia, United States of America
[5]Department of Biomedicine, University of Bergen, Bergen, Norway
[6]George A. Jervis Clinic, New York State Institute for Basic Research in Developmental Disabilities, Staten Island, New York, United States of America
[7]Research Design and Analysis Service, New York State Institute for Basic Research in Developmental Disabilities, Staten Island, New York, United States of America
[8]Department of Human Genetics, New York State Institute for Basic Research in Developmental Disabilities, Staten Island, New York, United States of America
[9]Center for Cardiovascular Research, Washington University School of Medicine, Saint Louis, Missouri, United States of America
[10]Center for Theragnosis, Korea Institute of Science and Technology, Seoul, Republic of Korea
[11]Department of Converging Science and Technology, KHU-KIST, Kyung Hee University, Seoul, Republic of Korea
[12]Department of Life Sciences, Pohang University of Science and Technology, Pohang, Republic of Korea
[13]Department of Biological Sciences, University of Bergen, Bergen, Norway
[14]Department of Surgery, Haukeland University Hospital, Bergen, Norway
[15]Department of Biochemistry and Biophysics, Perelman School of Medicine, University of Pennsylvania, Philadelphia, United States of America
[16]Biology PhD Program, The Graduate Center, The City University of New York, New York, United States of America
[17]Herman B. Wells Center for Pediatric Research, Indiana University School of Medicine, Indianapolis, United States of America
[#a]Current Address: Laboratory Animal Resource Center, Korea Research Institute of Bioscience and Biotechnology, Chungbuk, Republic of Korea

* Corresponding author

E-mail: minilee@kribb.re.kr / tinymini@ewhain.net (MNL)

gholsonjlyon@gmail.com / gholson.j.lyon@opwdd.ny.gov (GJL)

gootaeg@ewha.ac.kr (GTO)

¶These authors contributed equally to this work.

Abstract

There is an enormous amount of variation in proteins introduced by co- and post-translational modifications, including N-terminal acetylation (NTA), catalyzed by a set of N-terminal acetyltransferases (NATs). The NatA complex (including X-linked Naa10 and Naa15) is the major acetyltransferase, with 40–50% of all mammalian proteins being potential substrates. However, the overall role of NTA on a whole-organism level is poorly understood, particularly in mammals. Male mice lacking Naa10 show no globally apparent in vivo NTA impairment and, surprisingly, do not exhibit embryonic lethality. Rather Naa10 nulls display increased neonatal lethality, and the majority of surviving undersized mutants exhibit a combination of hydrocephaly, cardiac defects, homeotic anterior transformation (including an extra thoracic rib), piebaldism and urogenital anomalies. The lack of complete embryonic lethality in Naa10-null mice is explained by the discovery of Naa12, a previously unannotated Naa10-like paralogue with NAT activity that genetically compensates for Naa10. Mice deficient for Naa12 have no apparent phenotype, except for decreased fertility, whereas mice doubly deficient for Naa10 and Naa12 display embryonic lethality, thus presenting the complete machinery for NatA-mediated NTA in mouse development.

Introduction

N-terminal (Nt-) acetylation (NTA) is one of the most common protein modifications, occurring co- and post-translationally. Approximately 80% of cytosolic proteins are N-terminally acetylated in humans and ~50% in yeast (1), while NTA is less common in prokaryotes and archaea (2). NTA is catalyzed by a set of enzymes, the N-terminal acetyltransferases (NATs), which transfer an acetyl group from acetyl-coenzyme A (Ac-CoA) to the free α-amino group of a protein's N-terminus. To date, eight distinct NATs (NatA – NatH) have been identified in eukaryotes that are classified based on different subunit compositions and substrate specificities (3-5). NTA has been implicated in steering protein folding, stability or degradation, subcellular targeting, and complex formation (6-10). The vital role of NATs and NTA in development has also emerged (11).

NatA, the major NAT complex, targets ~40% of the human proteome, acetylating Ser-, Ala-, Gly-, Thr-, Val- and Cys N-termini after removal of the initiator methionine (1, 5). Human NatA consists of two main subunits, the catalytic subunit N-α-acetyltransferase 10 (NAA10) (Ard1) and the auxiliary subunit NAA15 (Nat1), and a regulatory subunit HYPK (12-14). NAA15 function has been linked to cell survival, tumor progression, and retinal development (15, 16). In addition, Naa10-catalyzed N-terminal acetylation has been reported to be essential for development in many species (11, 17-22), and although NatA is not essential in *S. cerevisiae*, depletion of *Naa10* or *Naa15* has strong effects, including slow growth and decreased survival when exposed to various stresses (23, 24).

NAA10 mutations were found to be associated with several human diseases characterized by severe phenotypes, including global developmental defects (11). Among these, the X-linked Ogden syndrome (OS) (25, 26) shows the most severe pathological features such as infant lethality and has reduced NatA catalytic activity. In a *Saccharomyces cerevisiae* model for the Naa10 Ser37Pro mutant, the mutation impairs NatA complex formation and leads to a reduction in NatA catalytic activity and functionality (27, 28). Further, OS patient-derived cells have impaired NTA *in vivo* of some NatA substrates (25).

Over the years, many additional pathogenic *NAA10* variants have been identified in *NAA10* (29-35) and the collection of presenting symptoms is currently referred to as Ogden syndrome or *NAA10*-related syndrome (36). Other families have also been identified with NAA15 mutations (29-35).

The autosomal *NAA10* homolog, *NAA11* (ARD2), has been reported to be present in mice and humans, and is co-expressed with *NAA10* in human cell lines (37). Therefore, *NAA11* could conceivably compensate when *NAA10* is reduced or lacking (11). However, *NAA11* was only found in testis and placenta in human and gonadal tissues in mouse, while *NAA10* showed widespread expression in various tissues in embryos and adults (38). Thus, any functional redundancy or compensation might be limited to certain tissues only.

To elucidate the functional role of *Naa10* during development in mice, we used two different *Naa10*-deficient mouse lines: one, referred to as *Naa10* knockout (KO), which was previously reported specifically related to bone density in postnatal day 3 (P3) mice (39), and another denoted as $Naa10^{tm1a(EUCOMM)Hmgu}$ ($Naa10^{tm1a}$), generated in this study. These *Naa10*-deficient mice exhibit pleiotropic developmental abnormalities at a range of different ages, overlapping with some of the phenotypes seen in human disease involving NAA10 impairment. Because we did not discover major changes in the overall Nt-acetylome in *Naa10* KO mice, we hypothesized that there might be a compensating gene in mice, which led us to the identification of a new paralog of *Naa10,* which we name *Naa12*. *Naa12* is expressed in several organs (liver, kidney, heart and testis) and, like Naa10, binds to Naa15 to mediate NatA activity. Furthermore, lethality was observed in *Naa10; Naa12* double-KO mice, which supports the compensatory role of *Naa12 in vivo*. Thus, we demonstrate that *Naa10* is essential for proper development and *Naa12*, a newly-identified paralog of *Naa10*, can play a compensatory role in mice.

Results

Naa10 knockout mice can be born, but display pleiotropic developmental defects

To explore the role of *Naa10* in development, most analyses were carried out using our *Naa10* KO model mice that had been generated previously (39) using a targeting vector deleting Exon1, including the start codon, and Exon2 to Exon4 containing the GNAT domain including the Acetyl-CoA binding motif, which is crucial for *Naa10* function. We also generated another *Naa10*-deficient mouse which we called $Naa10^{tm1a}$, expressing β-galactosidase rather than the *Naa10* gene (S1A Fig). *Naa10* expression was deficient in $Naa10^{tm1a}$ mice (S1B and S1C Fig). Especially strong β-gal staining was observed during embryonic stages in the brain, heart and spinal cord (S1D Fig). Male *Naa10* KO ($Naa10^{-/Y}$) embryos displayed mild to severe developmental defects compared to wild-type (WT) ($Naa10^{+/Y}$) embryos. Some $Naa10^{-/Y}$ mice had lower levels of somites and developmental delay. Additionally, some $Naa10^{-/Y}$ embryos had a normal number of somites but were retarded in growth (Fig 1A). Some of the embryos underwent lysis or remained arrested at an earlier stage than embryonic day 10.5 (E10.5), with no turning, an abnormal trunk, and underdeveloped facial features. These phenotypes also reproduced in $Naa10^{tm1a/Y}$ embryos. Next, we assessed whether *Naa10* is essential for viability and counted the Mendelian ratios. Both $Naa10^{-/Y}$ and $Naa10^{tm1a/Y}$ mice were under-represented after birth, while there was no significant reduction in the embryonic stage in both mouse lines (S1 and S2 Table). We monitored the pups daily at postnatal day 0 (P0) to postnatal day 3 (P3) and beyond, and the

survival rate of *Naa10*$^{-/Y}$ mice dramatically decreased relative to either WT (*Naa10*$^{+/Y}$ and *Naa10*$^{+/+}$) or heterozygous female (*Naa10*$^{+/-}$) mice after the first few days of life (Fig 1B), and a few *Naa10*$^{-/Y}$ mice with postnatal lethality exhibited severe developmental defects such as craniofacial anomaly, an undeveloped lower body, whole-body edema, and ocular malformations (Fig 1C).

Congenital heart defects are one of the main causes of infant lethality, and cardiac diseases are a common developmental anomaly in OS patients (31), with some OS males dying in infancy with cardiac arrhythmias (26). Therefore, we investigated whether *Naa10* KO affects cardiac development. Development of a four-chambered septated heart is normally complete at E14.5, therefore we examined the cardiovascular system at E14.5. We identified ventricular septal defects (VSD) in several *Naa10*$^{-/Y}$ embryos, as well as concomitant double outlet right ventricle (DORV) at E14.5 (Fig 1D, upper). Ventricular septal defects (VSD) and atrial septal defects (ASD) were also observed at E18.5 (Fig 1D, bottom), and persistent truncus arteriosus (PTA) or DORV, along with concomitant membranous and muscular VSDs, were found in several of the mice that died in the first day of life (n= 6/28 examined). Given the presence of outflow tract defects and VSDs, we examined whether the ductus arteriosus had closed appropriately or not at birth. Significantly, both *Naa10*$^{-/Y}$ and *Naa10*$^{-/-}$ females (n=3/28 examined) exhibited a patent ductus arteriosus, meaning there is a failure of the mutant *in utero* cardiovascular system to adapt to adult life (birth) and close the interatrial and aorta-pulmonary trunk shunts that are required for normal fetal life (40). As murine outflow tract and VSD defects are not compatible with postnatal survival (40), these data suggest that congenital heart defects in *Naa10*$^{-/Y}$ mice may explain some of their neonatal lethality (S2 Fig). We also examined surviving adult mice for any possible situs inversus, but we did not observe this in any adult (>4 weeks) *Naa10*$^{-/Y}$ mice examined (n=19). Combined, these data suggest that *Naa10* mutant CHDs are mainly confined to aberrant remodeling of the great vessels of the heart, leading to pulmonary overload at birth resulting in lethality.

Some of the surviving homozygous mice (*Naa10*$^{-/Y}$ and *Naa10*$^{-/-}$) had reduced body weight (Fig 2A). This reduced body weight continued through weaning, although some mice did lose weight as they developed progressive hydrocephaly. If the analysis was restricted to only include litters in which there was at least one *Naa10*$^{+/Y}$ and one *Naa10*$^{-/Y}$ mouse in the same litter alive to be weighed at P4 and beyond, it was consistently observed that the smallest weight animal among the two genotypes was almost always the *Naa10*$^{-/Y}$ mice. For example, 13 litters met this criteria from the mating (*Naa10*$^{+/-}$ x *Naa10*$^{+/Y}$), and 12/13 of the litters had the *Naa10*$^{-/Y}$ as the lower weight (Fisher's exact test, two-tailed, P value <0.0001). 5 litters met this criteria from the mating (*Naa10*$^{+/-}$ x *Naa10*$^{-/Y}$), and of these, all of them had the *Naa10*$^{-/Y}$ as the lower weight (Fisher's exact test, two-tailed, P value = 0.0079). Therefore, despite the known variability in weight data as a function of genetic background, environment, and stochastic variation (41), it does appear at least for "within-litter" analysis that *Naa10*$^{-/Y}$ males are born at a smaller weight than *Naa10*$^{+/Y}$ males and remain the smallest male in the litter throughout their life.

Although piebaldism has never been reported in humans with OS, all (100%) of *Naa10*$^{-/Y}$ and *Naa10*$^{tm1a/Y}$ mice exhibited hypopigmentation on their belly (Fig 2B, upper), with this piebaldism quite varied in its extent but not appearing to correlate in any way with other phenotypes, such as hydrocephaly. Another phenotype with complete penetrance was

181 bilateral supernumerary ribs (14 pairs of rib instead of 13) in all *Naa10*$^{-/Y}$ and *Naa10*$^{tm1a/Y}$
182 mice (Fig 2B, middle and bottom, Table 1). This extra pair of ribs linking to the sternum
183 transforms the T8 vertebrae into an anterior T7-like phenotype (S3A-S3D Fig, Table 1).

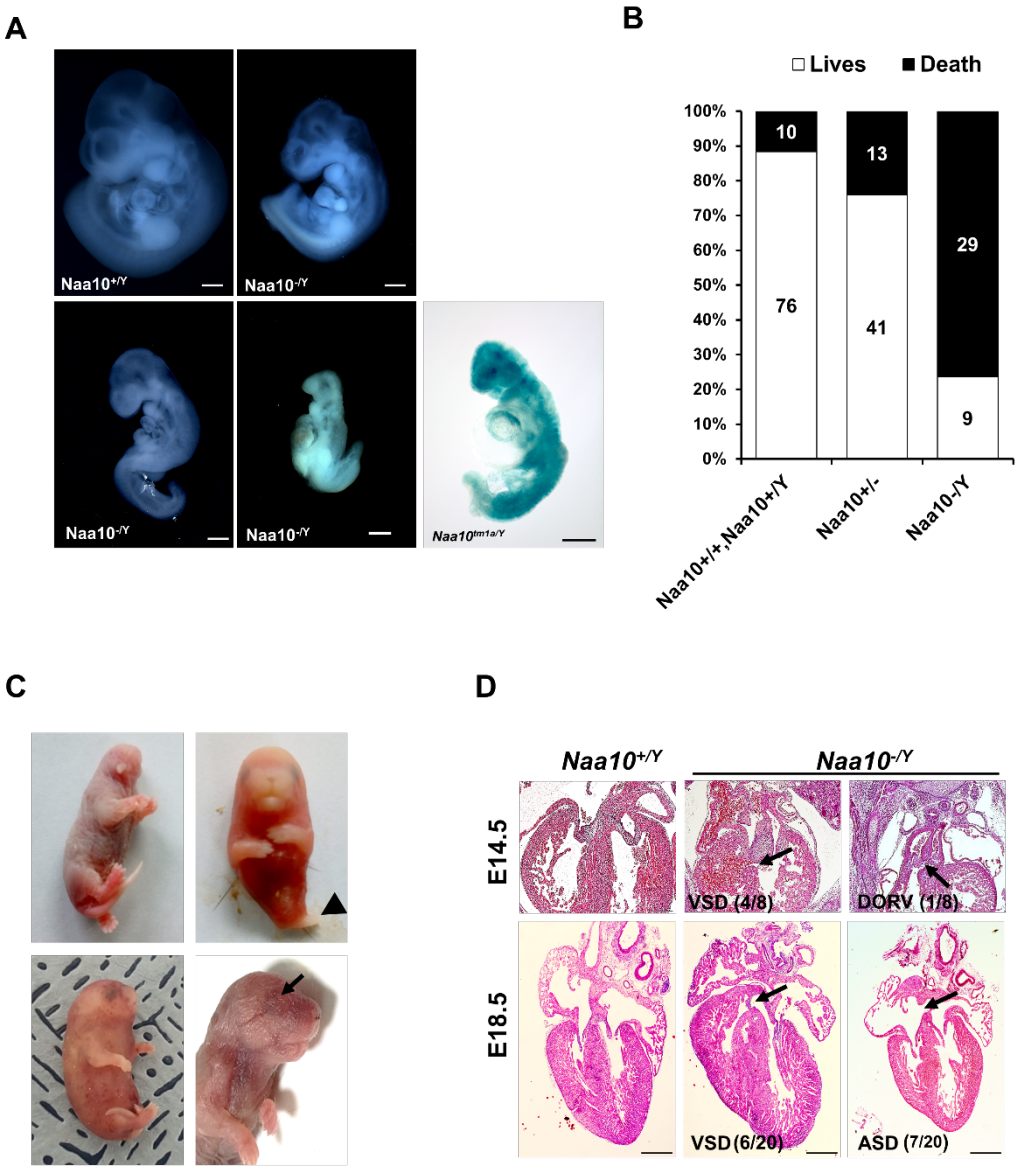

184 **Fig 1. Deficiency of *Naa10* leads to abnormal development and postnatal lethality.** (A) *Naa10*$^{+/Y}$,
185 *Naa10*$^{-/Y}$ and *Naa10*$^{tm1a/Y}$ embryos at E10.5. Growth retardation (5/33, more than 5 somites lower or
186 undersized compared to littermate controls), kinky trunk and developmental arrest are shown in
187 *Naa10*$^{-/Y}$ (4/33) and *Naa10*$^{tm1a/Y}$ (1/5). Scale bars: 500μm. (B) The percentage lethality in newborns,
188 comparing *Naa10* wild-type (*Naa10*$^{+/Y}$ and *Naa10*$^{+/+}$), *Naa10*$^{-/+}$ and *Naa10*$^{-/Y}$ pups until P3, derived
189 from matings between heterozygous females and wild-type (WT) males. Approximately 11.6%
190 (10/86) of WT, 24% (13/54) of *Naa10*$^{+/-}$ and 76.3% (29/38) *Naa10*$^{-/Y}$ mice were found dead before P3.
191 (C) Representative images of *Naa10*$^{-/Y}$ pups during early postnatal days compared with *Naa10*$^{+/Y}$.
192 Severe developmental defects such as malformations of head and lower body (one leg; black
193 arrowheads), whole-body edema and anophthalmia (black arrows) are shown (N=1 each). (D)
194 Hematoxylin and Eosin (H&E)-stained heart transverse section at E14.5 and vertical section at E18.5,
195 comparing *Naa10*$^{+/Y}$ and *Naa10*$^{-/Y}$ embryos. *Naa10*$^{-/Y}$ embryo shows a VSD at E14.5 and E18.5. Also,
196 at E18.5, *Naa10*$^{-/Y}$ embryo shows ASD. Arrow indicates VSD, ASD and DORV. Scale bars: 20 μm.
197 VSD, ventricular septal defect; ASD, atrial septal defect; DORV, double outlet right ventricle.

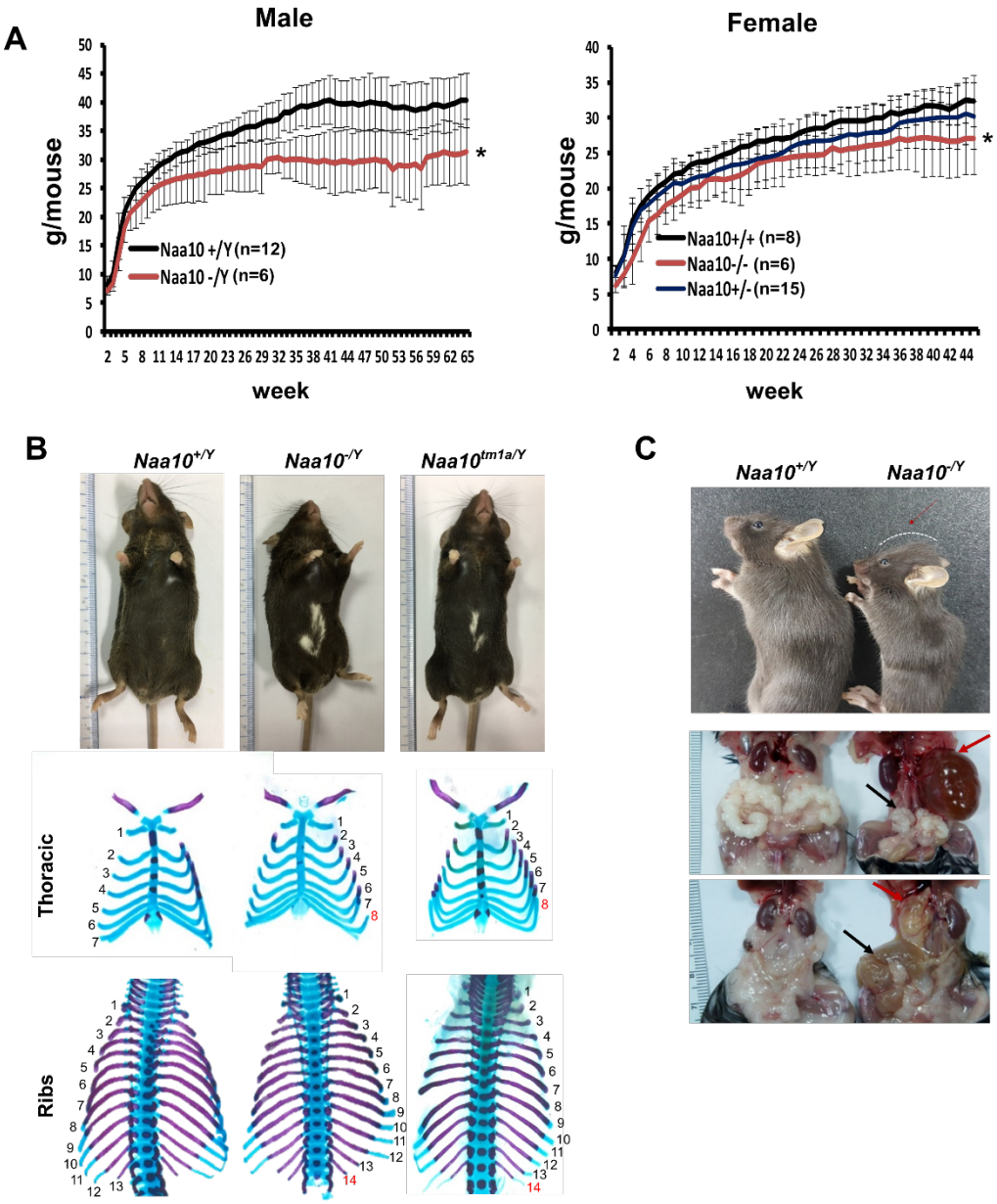

Fig 2. Pleiotropic phenotypes of *Naa10* KO mice. (A-C) Representative images of abnormalities in *Naa10*$^{-/Y}$ compared with *Naa10*$^{+/Y}$. (A) Body weight of male (left) and female (right) verses ages was monitored from 2 weeks. The weight of *Naa10*$^{-/Y}$ and *Naa10*$^{-/-}$ mice is markedly reduced compared with that of the WT mice. Asterisks indicate a statistical difference calculated by Student's *t*-test : *$p < 0.05$. (B) Representative images of completely penetrant phenotypes. Hypopigmentation (*Naa10*$^{+/Y}$, n=243; *Naa10*$^{-/Y}$, n=121; *Naa10*$^{tm1a/Y}$, n=17) and supernumerary ribs (*Naa10*$^{+/Y}$, n=3; *Naa10*$^{-/Y}$, n=6; *Naa10*$^{tm1a/Y}$, n=2; E18.5) were found 100% in *Naa10* deficient mice. (C) *Naa10*$^{-/Y}$ is smaller in size and has round-shaped head (*Naa10*$^{+/Y}$ 0/59, *Naa10*$^{-/Y}$ 7/33). Over time, hydrocephaly became apparent. (N=14/29 (~48%) for >P7 male *Naa10*$^{-Y}$; N=7/19 (~36%) for >P7 female *Naa10*$^{-/-}$). Hydronephrosis (red arrow, *Naa10*$^{+/Y}$ 0/23, *Naa10*$^{-/Y}$ 14/29, *Naa10*$^{+/+}$ 0/5, *Naa10*$^{-/-}$ 7/19) and abnormal genitalia (black arrow) of male (middle, *Naa10*$^{+/Y}$ 0/23, *Naa10*$^{-/Y}$ 16/29) and female (bottom, hydrometrocolpos, *Naa10*$^{+/+}$ 0/5, *Naa10*$^{-/-}$ 7/19) are shown.

213 **Table 1. Skeletal analyses for ribs, sternebrae, and vertebrae**

	Naa10$^{+/Y}$ (n=50)	Naa10$^{+/+}$ (n=10)	Naa10$^{+/-}$ (n=17)	Naa10$^{-/Y}$ (n=17)	Naa10$^{-/-}$ (n=1)
sternebrae	7 (14.0%)	1 (10%)	3(17.6%)	9 (52.9%)	1 (100%)
3 sternebrae	27 (54.0%)	8 (80%)	11(64.7%)	5 (29.4%)	0 (0%)
4 sternebrae but with 3/4 fusion	16 (32%)	1 (10%)	3 (17.6%)	3 (17.6%)	0 (0%)
14 ribs total bilaterally	0 (0%)	0 (0%)	0 (0%)	17 (100%)	1 (100%)
13 ribs total bilaterally	50 (100%)	10 (100%)	17 (100%)	0 (0%)	0 (0%)
8 ribs attached to sternum bilaterally	0 (0%)	0 (0%)	0 (0%)	17 (100%)	1 (100%)
7 ribs attached to sternum bilaterally	50 (100%)	10 (100%)	17 (100%)	0 (0%)	0 (0%)
14 Thoracic vertebrae	0 (0%)	0 (0%)	0 (0%)	17 (100%)	1 (100%)
13 Thoracic vertebrae	50 (100%)	10 (100%)	17 (100%)	0 (0%)	0 (0%)

214 Tabulation regarding the number of sternebrae found in skeletons, including ones in which there was
215 partial fusions between the 3rd and 4th sternebrae.

216

217 A majority of the *Naa10*$^{-/Y}$ and *Naa10*$^{-/-}$ mice also had four instead of the usual three
218 sternebrae, which were sometimes fused (Table 1). Cervical vertebrae fusion was also
219 demonstrated in *Naa10*$^{-/Y}$ mice, particularly involving C1 and C2, suggesting possible
220 anteriorization of C2 into a C1-like phenotype (S3E and S3F Fig, and Table S3). The number
221 of lumbar vertebrae remained the same, thus suggesting an anterior transformation of the first
222 sacral vertebra to a lumbar-like phenotype. These combined observations suggest possible
223 anterior transformations in the *Naa10* mutant skeletal phenotype, with an anteriorization of
224 C2, a T8 transformation to a T7-like phenotype with ribs connecting to the sternum, an extra
225 pair of ribs on L1 likely due to an L1 transformation to a T13-like phenotype, and an anterior
226 transformation of the first sacral vertebra to a lumbar-like phenotype with loss of fusion to
227 the sacral wings.

228 Some *Naa10* KO (*Naa10*$^{-/Y}$ and *Naa10*$^{-/-}$) mice survived more than 4 months, with
229 some of these then developing hydronephrosis (Fig 2C, middle). They had some hollowed
230 space in the kidney, which had been filled with fluid and their ureter was thickened already at
231 P3 stage of prenatal development in some *Naa10*$^{-/Y}$ mice (S4A Fig). Commonly,
232 hydronephrosis is caused by a blockage or obstruction in the urinary tract. We speculate that
233 this swelling in *Naa10* KO (*Naa10*$^{-/Y}$ and *Naa10*$^{-/-}$) mice is likely caused by ureteral defects
234 rather than the kidney itself. Moreover, some *Naa10* KO mice displayed genital defects, such
235 as seminal vesicle malformation and hydrometrocolpos, respectively (Fig 2C, bottom). Many
236 *Naa10*$^{-/-}$ female mice appeared to have decreased fecundity, although they were fertile upon
237 the first mating, and this decrease in fecundity is possibly due to the development of
238 hydrometrocolpos (Fig 2C, bottom), which might result from structural issues, like vaginal
239 atresia or a retained vaginal septum, although this requires further investigation. Additionally,
240 hydrocephaly became clinically apparent with a round-shaped head (Fig 2C, upper) in some
241 *Naa10*$^{-/Y}$ mice. CT scanning of some of these mice confirmed hydrocephaly as the primary
242 cause of their rapid deteriorating condition, usually within the first 3 months of life (S4B
243 Fig). CT scanning did not reveal any obstructive lesions (such as a tumor) in any of the

ventricles that could account for the hydrocephaly. Taken together, these results indicate that *Naa10* contributes to overall development and is particularly important for viability.

Litter sizes and offspring from other matings were also investigated, as shown in Table S4. Matings were set up between *Naa10*$^{-/-}$ females and C57bl6J WT (*Naa10*$^{+/Y}$) males, involving eleven mating pairs with 7 unique females and 7 unique males. Of a total of 127 pups that were born, 37 died in the first day of life and were degraded and/or cannibalized prior to any tail sample being retrieved, thus not being genotyped. This was a relatively high death rate in the first 24 hours of life (29%), more so than with the other matings, except for the one between *Naa10*$^{-/-}$ females and *Naa10*$^{-/Y}$ males (Table S4). However, this is substantially less than the death rate of 90% (46/51) reported for the same mating in the Lee *et al.* paper (42), and we currently do not have an explanation for this discrepancy. Of the remaining 90 pups that could be genotyped, 59 of these were *Naa10*$^{+/-}$ females and 31 were *Naa10*$^{-/Y}$ males. Seven of the 59 *Naa10*$^{+/-}$ females and two of the 31 *Naa10*$^{-/Y}$ males died in the first 3 days of life (for a total death rate in the first three days for all born pups of 46/127, or 36%), and after this time, none of the remaining *Naa10*$^{+/-}$ females died in the first ten weeks of life (88% overall survival), whereas ten of the 31 *Naa10*$^{-/Y}$ males developed hydrocephaly and died in the first ten weeks of life (61% overall survival). The death rate of 36% in the first three days of life is similar to the rate of 42.4% seen with the mating of *Naa10*$^{-/-}$ females with *Naa10*$^{-/Y}$ males (Table S4), whereas this rate is higher than that seen for *Naa10*$^{+/-}$ females with *Naa10*$^{+/Y}$ males (15.8%) and *Naa10*$^{+/-}$ females with *Naa10*$^{-/Y}$ males (13.6%).

***Naa10*-deficient mice have a functionally active NatA complex**

OS shows reduced *in vivo* protein Nt-acetylation in patient cells (25). Reduced Nt-acetylomes were also observed in the *Naa10* mutant yeast models (27). Given these prior reports, we hypothesized that pleotropic phenotypes in *Naa10*-deficient mice are due to a decrease in global N-terminal acetylation. To test our hypothesis, integrated N-terminal peptide enrichment method (iNrich) (43) was used to analyze the level of protein Nt-acetylation in mouse embryonic fibroblasts (MEFs) of *Naa10*$^{+/Y}$ and *Naa10*$^{-/Y}$. To evaluate the degree of Nt-acetylation, we applied a mass spectrometry (MS)-based N-terminomics method to protein lysates from MEFs. Since the samples are treated with deuterated acetic anhydride prior to MS, unacetylated N-terminal site appears with +3 Da mass shift in the MS spectrum of the corresponding acetylated N-terminal site (44). The peak intensity ratios of acetyl/heavy acetyl pairs represent degree of acetylation of the N-terminal site. We found 765 acetyl/heavy acetyl pairs of N-termini throughout five replicates of *Naa10*$^{+/Y}$ and five replicates of *Naa10*$^{-/Y}$. Except for the sites detected only in either WT or mutant, 533 N-terminal sites could be compared. Approximately 98% (n=523) of N-termini pairs showed less than 10% variation in the degree of Nt-acetylation, indicating that there is no significant difference in Nt-acetylation between *Naa10*$^{-/Y}$ and *Naa10*$^{+/Y}$ mice (Fig 3A). To further investigate this, we measured the *in vitro* Nt-acetylation activity of NatA via immunoprecipitation of the large auxiliary subunit Naa15 from mouse tissues. This analysis showed normal expression of Naa15 in *Naa10* KO liver tissue as in WT tissues (Fig 3B), and we isolated a physical complex composed of Naa15 and undefined partners that retains NatA activity from *Naa10* KO tissues (Fig 3C). These data suggest that despite the loss of *Naa10* in mice, the NatA complex remains active.

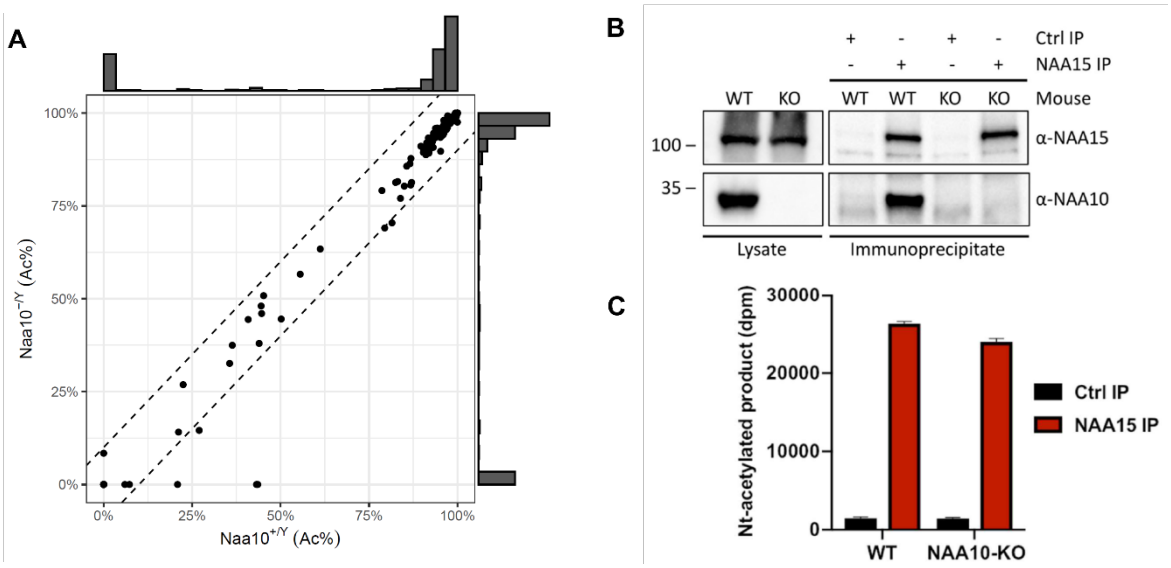

Fig 3. Activity measurement of NatA from WT and *Naa10* KO mice. (A) Correlation of Naa10 alteration state on Nt-acetylation in mouse embryonic fibroblasts (MEFs). Each dot (n=533) represents the average Nt-acetylation percentage of 5 replicates of *Naa10*$^{+/Y}$ and *Naa10*$^{-/Y}$, respectively. Dashed lines are the borders of ±10% difference. Except for the ten dots, 523 of the 533 dots are within the borders. The marginal histograms show the distribution of Nt-acetylation data points. (B) Immunoprecipitation of Naa15. Liver tissue from WT and *Naa10* KO mouse was lysed and incubated with anti-Naa15 antibody to retrieve NatA complexes. Proteins were separated by SDS-PAGE and immunoblots probed with anti-Naa15 antibody and anti-NAA10 antibody. (C) Catalytic activity of immunoprecipitated NatA. The catalytic activity of NatA precipitated from WT and *Naa10* KO mouse liver tissue by anti-Naa15 was measured towards the NatA substrate peptide $SESS_{24}$ in an *in vitro* [^{14}C]-Ac-CoA–Based Acetylation Assay. Control reactions were performed with no enzyme or no peptide to account for background signal. The immunoprecipitation (IP) and activity measurements were performed in three independent setups, each with three technical replicates per assay. One representative setup is shown.

A *Naa10* paralog exists in mice

Naa10 disruption is lethal in a variety of organisms, including *D. melanogaster* (17), *C. elegans* (18) *and T. brucei* (45). Given the relatively mild phenotype and no reduction of the Nt-acetylome in *Naa10* KO mice, we hypothesized that there might be a yet unidentified paralog of *Naa10,* which can compensate for loss of function in mice. A Blast search for genomic sequences with homology to *Naa10* exposed several *Naa10* pseudogenes on chromosome 2, 3, 7, 12, 15 and 18. Additionally, southern blot analysis from C57BL/6J DNA with *Naa10* cDNA probe detected bands of the expected sizes on the X chromosome (S5A and S5B Fig), while other bands of unexpected sizes appeared on other chromosomes 2, 5, 15 and 18. The previously identified *Naa10* paralog *Naa11* is located on chromosome 5, however, this paralog is only expressed in testes (38). We identified a homologous sequence on chromosome 18, which we named *Naa12*. This predicted gene shows high similarity to *Naa10,* and RiboSeq and mRNA traces of this region suggest possible transcription and translation of this gene (S5C Fig). The protein sequence of *Naa12* is >80% identical to *Naa10*. In addition, *Naa12* is almost 90% identical with *Naa11* (37).

319 Quantitative PCR (q-PCR) analysis also confirmed the expression of this transcript in
320 all tested tissues (S6A Fig), with the expression of Naa12 unchanged in the corresponding
321 *Naa10* KO tissues. We performed a sequence alignment of the two known mNaa10 isoforms,
322 mNaa11 and mNaa12 and selected a unique Naa12 peptide for immunization and antibody
323 generation (S6B Fig). After generation and affinity-purification, we validated the specificity
324 and sensitivity of this Naa12 antibody (S6C and S6D Fig). Western blot analyses from mouse
325 tissue demonstrated a band at around 35 kDa in both kidney and heart lysates, while we could
326 not detect Naa12 in liver (S6E Fig). To assure that the antibody is specific, we also probed the
327 membrane with Naa12 antibody that was blocked by the peptide it was raised against. The
328 band at 35 kDa disappears when probed with the blocked antibody, which appears to confirm
329 the specificity.

330 To test whether Naa12 has a similar enzymatic activity as Naa10, we performed a
331 radioactive-based acetyltransferase assay using synthetic peptides (Fig 4A). Since
332 monomeric Naa10 preferentially acetylates N-termini with acidic side chains (46-48), we
333 used peptides representing the N-termini of γ -actin (starting DDDIA-) and γ-actin (starting
334 EEEIA-), the two known Naa10 in vitro substrates. Additionally, we used a peptide starting
335 with SESSSKS-, an in vitro NatA complex substrate High mobility group protein A1. As
336 expected for the monomeric proteins, we could not detect any activity towards the SESSSKS-
337 substrate. Importantly, both Naa10 and Naa12 significantly Nt-acetylated the acidic N-
338 terminal peptides demonstrating the intrinsic capacity of Naa12 to catalyze Nt-acetylation
339 (Fig 4A).

340 Across species, Naa10 is bound to its auxiliary subunit, Naa15, which links the
341 catalytic subunit to the ribosome to facilitate co-translational Nt-acetylation of proteins as
342 they emerge from the exit tunnel (23, 49-53). Due to its high sequence similarity (see also
343 S4B Fig), we suspected that Naa12 may also interact with Naa15. To test this hypothesis, we
344 performed co-immunoprecipitation assays in HEK 293 cells. Apart from Naa10 (isoform 1,
345 $Naa10^{235}$) and Naa12, we also included the second isoform of mNaa10, $mNaa10^{225}$ that has
346 been described earlier (12, 50, 54) as well as Naa11. Both Naa10 isoforms as well as Naa11
347 and Naa12 co-precipitated with V5-Naa15 but not V5 alone, suggesting that all tested
348 proteins could form a stable complex with Naa15 in mouse (Fig 4B). In a mass spectrometry
349 analysis of a similar setup to that shown in Fig 3B, immunoprecipitation of endogenous
350 Naa15 from liver tissue derived from WT and Naa10 KO mice, we identified one peptide in
351 the Naa10 KO sample that is identical between Naa12 and Naa11, but differing from Naa10
352 (Table 2). Further, we detected a number of peptides shared between Naa10, Naa11 and
353 Naa12 in the Naa15 immunoprecipitates from the Naa10 KO sample. In contrast, peptides
354 unique for Naa10 were only detected in the WT mouse sample. This together with data
355 demonstrating that Naa11 is only expressed in testes and that no Naa10 is present in the
356 Naa10 KO mice, strongly suggest that endogenous Naa15-Naa12 complexes are present in
357 Naa10 KO mice.

A

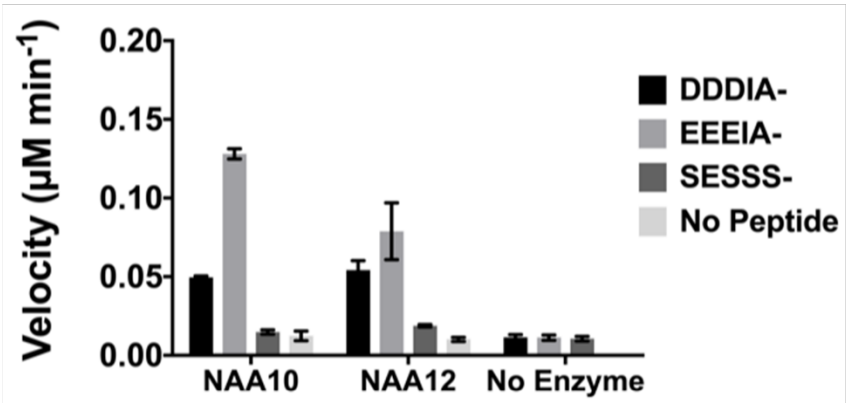

B

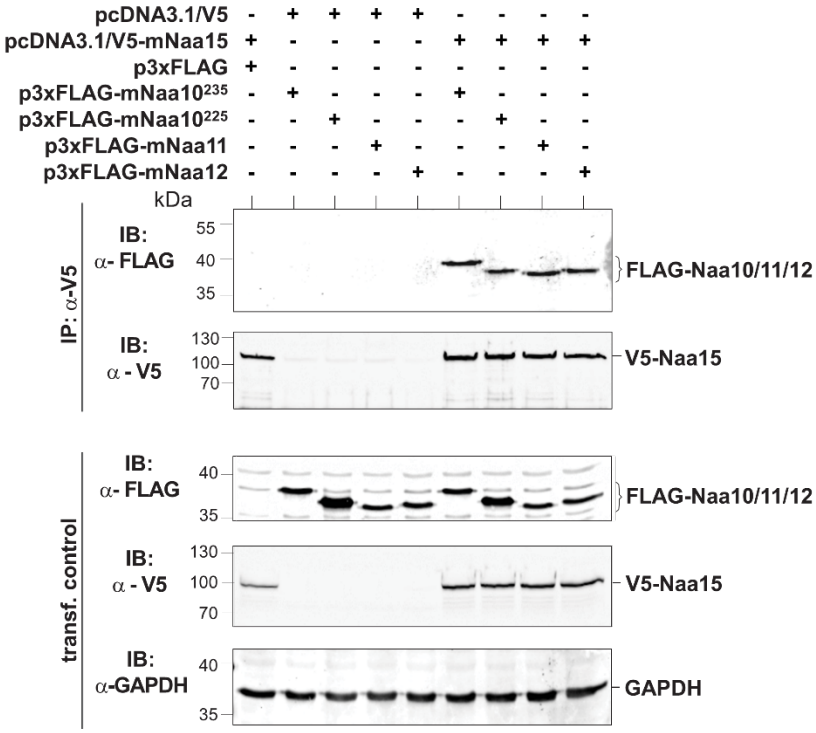

358

359 **Fig 4. Characterization of *Naa12.*** (A) In vitro N-terminal acetyltransferase radioactive-based assay.
360 Comparison of mouse Naa10 and Naa12 towards Naa10 peptide substrates, beta-actin (DDDIA-) and
361 gamma-actin (EEEIA-), and the optimal NatA complex peptide substrate, SESSS-. Background
362 control reactions were performed in the absence of either peptide or enzyme. Assays were performed
363 in triplicate; error bars represent S.E.M. (B) Co-immunoprecipitation assay. HEK293 cells were
364 transfected as indicated and lysed after 48 h. Cell lysates were incubated with 1 μg anti-V5 antibody
365 to precipitate V5-tagged Naa15. The isolated complexes were separated on SDS-PAGE and probed
366 with the indicated antibodies.
367

368

369 **Table 2. Naa10, Naa11 and Naa12 peptides identified by LC-MS/MS analysis in Naa15 IP samples**
370 **from WT and *Naa10* KO mouse**

Gene name	Peptide sequence	Log 2 intensity	
		WT mouse*	*Naa10*-KO mouse*
Naa11/Naa12	AALHLYSNTLNFQVSEVEPK	23,4375	26,1335
Naa10/Naa11/Naa12	IVGYVLAK	27,0429	24,5347
Naa10/Naa11/Naa12	MEEDPDDVPHGHITSLAVK	27,7220	28,6816
Naa10/Naa11/Naa12	MEEDPDDVPHGHITSLAVKR	24,5443	24,0103
Naa10/Naa11/Naa12	YVSLHVR	22,5860	22,5039
Naa10/Naa11/Naa12	YYADGEDAYAMK	26,1440	25,9763
Naa10/Naa11/Naa12	YYADGEDAYAMKR	26,1874	25,9960
Naa10	AMIENFNAK	26,3537	-
Naa10	DLTQMADELRR	24,4664	-
Naa10	GNVLLSSGEACREEK	24,9817	-
Naa10	HMVLAALENK	24,4828	-
Naa10	NARPEDLMNMQHCNLLCLPENYQMK	25,0599	-
Naa10	YYFYHGLSWPQLSYIAEDENGK	26,7277	-

371 *Samples were run in technical duplicates and the average log2 intensity of the peptides are presented.

372

373 ***Naa12* may rescue loss of *Naa10* in mice**

374 To investigate whether *Naa12* can rescue the loss of the function of Naa10 *in vivo*,
375 *Naa12* KO mice were generated using CRISPR technology (55). One 95-base pair deletion
376 Δ131-225 in *Naa12* was characterized in depth (Fig 5A). This mutation introduces a
377 frameshift, leading to a termination codon at amino acid 67, which should either result in
378 complete knockout of the protein or, at best, the expression of a truncated mini-protein that
379 would be far shorter than the usual 220 amino acid Naa12. We confirmed the deletion by
380 PCR with genomic DNA (Fig 5B). QPCR further showed deletion of *Naa12* in the tested
381 tissues of *Naa12* KO mice (Fig 5C), however, it seemed that *Naa12* might be slightly
382 expressed in testis. Due to the high similarity between *Naa11* and *Naa12*, the expression
383 shown in *Naa12* KO testis could actually be *Naa11* rather than *Naa12*, and this was
384 confirmed by RT-PCR showing definite deletion (S7A Fig). This was confirmed at the protein
385 level with the Naa12 antibody in heart tissue lysates (S7B Fig). However, this antibody was
386 unable to consistently detect protein even in WT liver, kidney, or brain tissue lysates, which
387 could be due to very low expression or post-translational modification of Naa12 in these
388 tissues. Furthermore, given that this antibody is raised against a peptide at the C-terminus of
389 Naa12, these results do not completely exclude the possibility of truncated non-functional
390 mini-protein expression, although the lack of any signal with RT-PCR (S7A Fig) likely means
391 that nonsense-mediated decay occurred.

392

393

394

395

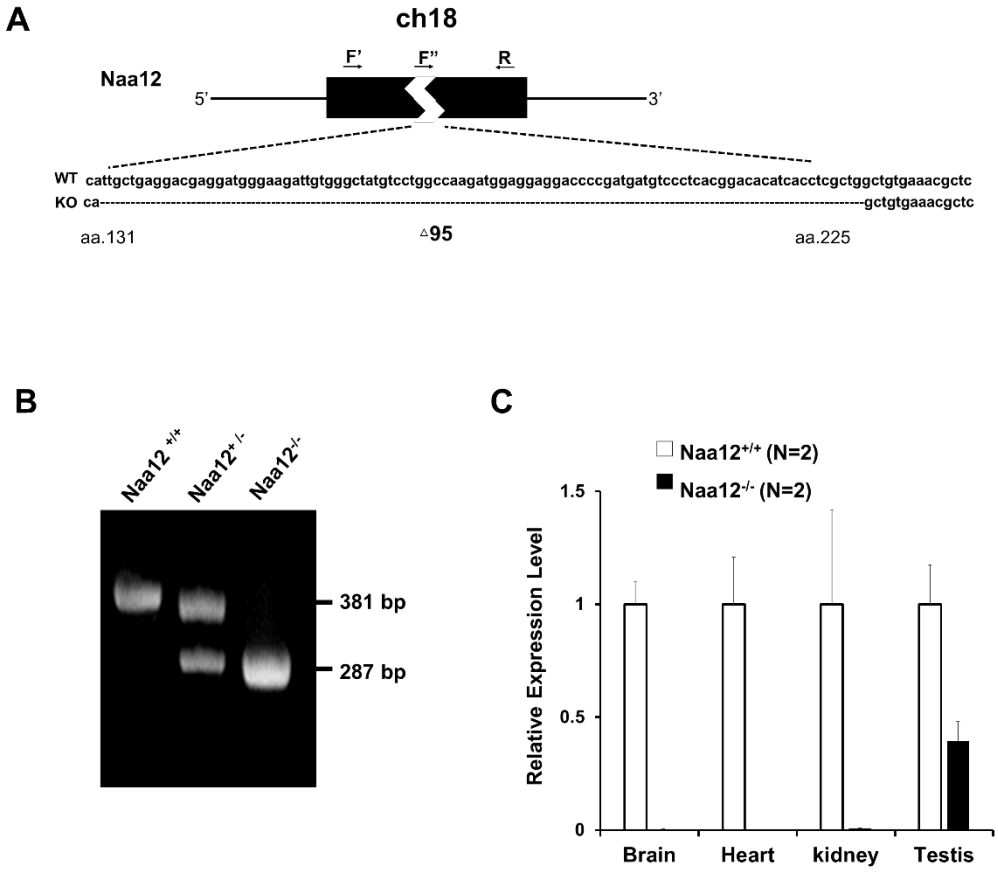

Fig 5. Generation of *Naa12* KO mice. (A) Scheme of *Naa12* deletion used to generate *Naa12* KO mouse. 95 base pairs (131-225) were deleted. F'; genomic DNA forward primer, F"; cDNA forward primer, R; reverse primer. (B) Genotyping of *Naa12* KO mice by PCR. WT allele size was 381bp and targeted allele size was 287bp. (C) mRNA level of *Naa12* were analyzed in selected tissues by qPCR. Relative expression level of WT (white bars) and *Naa12* KO (black bars) after normalizing to that of GAPDH.

Homologs that play a compensatory role usually show similar phenotypes to each other when one of them is deficient (56). Therefore, we analyzed *Naa12* KO mice to see if they produced similar developmental defects to those in *Naa10* KO mice. Unexpectedly, knockout mice for this gene were viable (Table S5), albeit at a reduced rate of fertility (Table S4). Necropsy and inspection of testes and seminal vesicles under a stereomicroscope, along with weighing these tissues, did not reveal any macroscopic differences that could readily explain the decreased fertility of the *Naa12 KO* males. Furthermore, the phenotypes (piebaldism and bilateral supernumerary ribs; Fig.2b) observed in *Naa10* KO mice with complete penetrance were not present in *Naa12* KO mice (S7C Fig). Overall, there were not any obvious phenotypes in these mice, except for reduced fertility.

Matings between compound heterozygous ($Naa10^{+/-}$; $Naa12^{+/-}$) females and $Naa10^{+/Y}$; $Naa12^{+/-}$ males demonstrate that no live births occurred for *Naa10; Naa12* double-knockout (DKO) males ($Naa10^{-/Y}$; $Naa12^{-/-}$) (Fig 6A). In addition, the average litter size was

very small when compared to the control (WT x WT) matings, suggesting embryonic lethality (Table 3 and Table S4). In order to determine whether lethality occurs during the embryonic stage, we genotyped E18.5 litters – just before birth. Consistent with our previous observations, we could not obtain any *Naa10*$^{-/Y}$; *Naa12*$^{-/-}$ embryos, and many embryos could not be genotyped because they were already in the midst of resorption (n=23) (Fig 6). We checked an even earlier stage at E10.5 and also found zero *Naa10*$^{-/Y}$; *Naa12*$^{-/-}$ embryos, and also with far fewer resorptions at this stage (N=3). Interestingly, we did observe *Naa10*$^{-/Y}$; *Naa12*$^{+/-}$ embryos where two of them displayed delayed developmental stage (appearing younger than E10.5) and another two embryos were lysed and had already begun degenerating (but despite this, we could at least genotype these embryos). This helps explain why only one *Naa10*$^{-/Y}$; *Naa12*$^{+/-}$ embryo was observed at E18.5. Furthermore, *Naa10*$^{+/-}$; *Naa12*$^{-/-}$ female embryos were also lysed/degenerating at E10.5 and were not observed from that day onward. Matings between compound heterozygous females and *Naa10*$^{+/Y}$; *Naa12*$^{-/-}$ males also did not yield *Naa10*$^{-/Y}$; *Naa12*$^{-/-}$ male or *Naa10*$^{+/-}$; *Naa12*$^{-/-}$ female mice during development (S8 Fig). Consistent with our previous findings, we noted many resorptions at E12.5 and E18.5 that could not be genotyped. The number of living postnatal compound heterozygous female mice was also considerably lower than the predicted Mendelian ratios (Fig. 6 and S8 Fig), and the surviving *Naa10*$^{+/-}$; *Naa12*$^{+/-}$ females were smaller in size than littermate controls (Fig. 7D). Due to the severe embryonic lethality observed in the *Naa10; Naa12* DKO male mice and the *Naa10*$^{+/-}$; *Naa12*$^{-/-}$ female mice, which was not seen in each single KO (*Naa10* KO or *Naa12* KO), it seems likely that, without compensation by Naa12, NTA is disrupted in *Naa10; Naa12* DKO mice. Together, these data support the compensatory role of Naa12 *in vivo*.

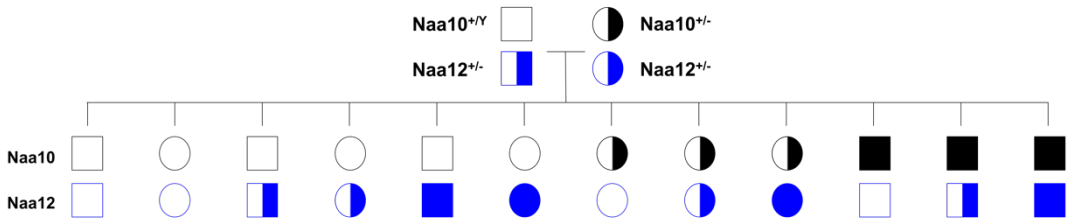

Genotype	Naa10$^{+/Y}$ Naa12$^{+/+}$	Naa10$^{+/+}$ Naa12$^{+/+}$	Naa10$^{+/Y}$ Naa12$^{+/-}$	Naa10$^{+/+}$ Naa12$^{+/-}$	Naa10$^{+/Y}$ Naa12$^{-/-}$	Naa10$^{+/+}$ Naa12$^{-/-}$	Naa10$^{+/-}$ Naa12$^{+/+}$	Naa10$^{+/-}$ Naa12$^{+/-}$	Naa10$^{+/-}$ Naa12$^{-/-}$	Naa10$^{-/Y}$ Naa12$^{+/+}$	Naa10$^{-/Y}$ Naa12$^{+/-}$	Naa10$^{-/Y}$ Naa12$^{-/-}$	Unable to genotype
E10.5 (n=29)	1	2	1	4	3	3	3	6	2†	0	4*†	0	3
E18.5 (n=33)	4	5	5	7	3	1	1	5	0	1	1	0	23
Postnatal (n=157)	17	16	31	28	17	16	14	5	0	13	0	0	0

* delayed embryonic days
† lysed embryo

Fig 6. Lethality in *Naa10*; *Naa12* DKO mice. (A) *Naa10*; *Naa12* DKO exhibit embryonic lethality. Pedigree and genotypes of pups and embryos at E10.5 and E18.5 from *Naa10*$^{+/-}$; *Naa12*$^{+/-}$ female mice crossed to the *Naa10*$^{+/Y}$; *Naa12*$^{+/-}$ male mice.

Table 3. Litter size of Naa10;Naa12 DKO matings

Genotypes of Naa10; Naa12 breeders (♀ x ♂)	Total number of pups	Total number of litters	Average litter size (pups/litters)	SD of litter size
Naa10$^{+/+}$; *Naa12*$^{+/+}$ x *Naa10*$^{+/Y}$; *Naa12*$^{+/+}$	206	24	8.6	1.6
Naa10$^{+/-}$; *Naa12*$^{+/-}$ x *Naa10*$^{+/Y}$; *Naa12*$^{+/-}$	157	32	4.9	1.5

SD : Standard Deviation

Statistical examination of weight data in *Naa10*- and *Naa12*-deficient mice

To determine whether Naa10 and Naa12 are essential for viability and development, we examined the survival, weights, and growth rates of 688 *Naa10* and *Naa12* knockout and wild type mice. The genotypes of mice examined are listed in Table S6. To avoid potential survival biases, only weights taken during the first 180 days were included. Growth curves are shown in Fig 7. Age and age-squared (the quadratic term) are both entered in the analyses; the quadratic term shows the degree to which the effect of age itself changes with age.

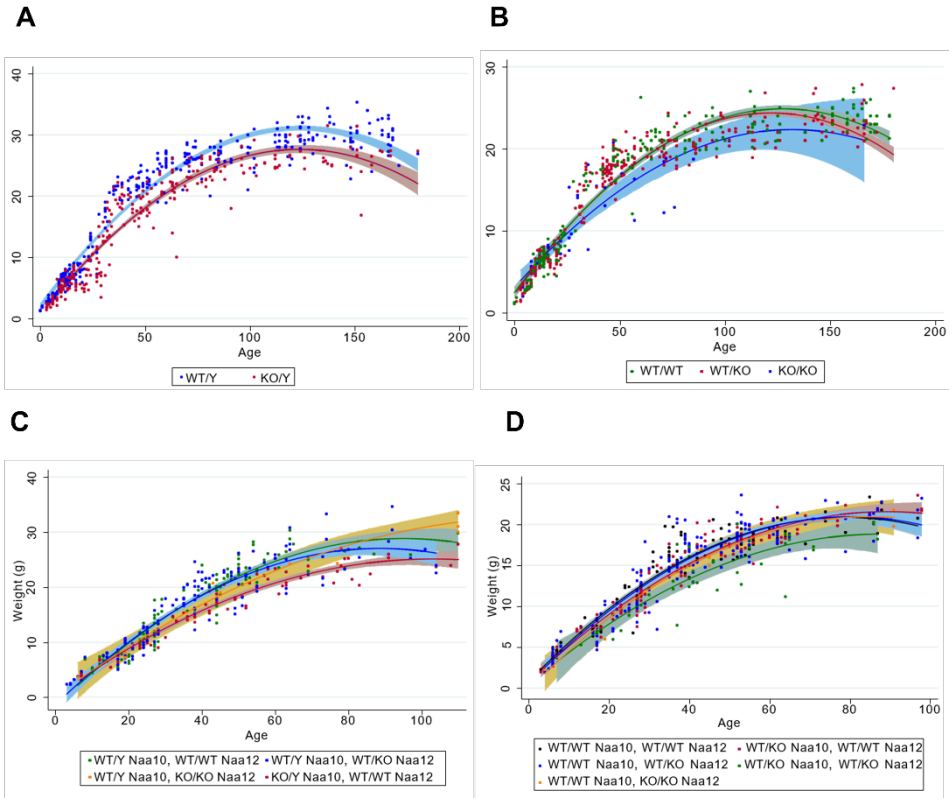

Fig 7. Decreased body weight in compound heterozygous females. (A) Male body weight for the *Naa10* mice on inbred genetic background (8 backcrosses to C57bl6/J). (B) Female body weight for the *Naa10* mice on inbred genetic background (8 backcrosses to C57bl6/J). (C) Male body weight for the *Naa10* and *Naa12* mice on mixed genetic background. (D) Female body weight for the *Naa10* and *Naa12* mice on mixed genetic background.

Table S7 shows the results in which weight of *Naa10* mice in grams is regressed upon age, Naa10 knockout status, and their interaction. Unsurprisingly, age predicts weight for males and females strongly, with growth slowing with age (first column). Though a strong negative effect of the knockout is seen in for both males and females (second column), when both age and knockout status are modeled together (third column) this effect all but disappears in females. Moreover, in females there is no interaction of knockout status with age (fourth column), suggesting that the *Naa10* knockout status itself has no significant effect on the growth rate in females. For males, however, the main effect of the knockout remains when age is included in the model (third column) and the interaction is significant (fourth column), indicating that the *Naa10* knockout both reduces weight of males overall and lowers the rate of growth.

Results of analyses of mixed-genetic background *Naa10/Naa12* mice are shown in Table S8. Effects of age and knockouts on weight comprise the upper portion of the table, while the lower portion shows their effect on the rate of weight gain. Among females a significant reduction of weight (above, second column) and in the rate of growth (below, first column) is seen among mice heterozygous for the *Naa10* KO. There were no homozygous *Naa10* KO female mixed-breed mice available to analyze, as the matings were not set up to yield any such mice (so breeding patterns, not mortality in utero, are the reason for this absence). No significant effect on growth rate is seen for heterozygous or homozygous *Naa12* KO (above, third column) or for their interactions with age (below, second column), and only the effects of the heterozygous *Naa10* KO and its interaction with age are seen in the full model (below, third column). Thus the *Naa12* KO, whether heterozygous or homozygous, does not appear to reduce the weight or growth rate of females, while a heterozygous *Naa10* KO is sufficient to reduce both weight and growth rate. Interestingly, when modeled together, both the Naa10 and the *Naa12* KOs significantly reduced weight (above, fourth column) and the interaction of the Naa10 and the *Naa12* heterozygous KOs significantly reduced weight (above, fifth column). As no female mice were both KO for *Naa10* and homozygous KO for *Naa12*, the effect of the interaction of those two factors could not be determined. The triple interaction of heterozygous *Naa10* KO, *Naa12* KO and age was weakly significant, suggesting that the presence of both knockouts affects growth rate above and beyond the effects of each knockout independently (below, fourth column). No males with knockouts of both *Naa10* and *Naa12* were born, so no test of their interaction was possible. An effect was seen for the Naa10 knockout on weight when modeled with age and age^2 (second column), and the significant interaction of the *Naa10* knockout with age and age^2 (third column) shows that the *Naa10* KO in males reduces the growth rate. As with females, no significant effect of a *Naa12 KO*, whether heterozygous or homozygous, was seen in males, nor is there a significant interaction with age (fourth column). When the interactions of age with both *Naa10* and *Naa12* knockout status are entered in one model, *Naa10* alone is seen to reduce growth rates (fifth column).

Discussion

We have shown that Naa10 deficiency results in pleotropic developmental defects in two different Naa10-deficient mouse models. Similar to infant mortality in some OS males, the lethality of *Naa10* KO mice increased dramatically in pups in the first 3 days of life (Fig 1B). Defects in kidney, brain, pigmentation (piebaldism), and ribs were observed during embryonic or early postnatal stages in some mice (Fig 2B and 2C). These observed

508 phenotypes overlap with some of the phenotypes found in surviving humans with OS,
509 including supernumerary vertebrae and hydrocephaly, although piebaldism has not been
510 reported to date in any humans. However, the puzzling lack of embryonic lethality in the
511 *Naa10* KO mice prompted us to discover *Naa12* as a possible compensatory NAT, with
512 Naa10-like NTA activity (Fig 4A), with an interaction between Naa15 and Naa12 (Fig 4B). In
513 addition, co-immunoprecipitation of endogenous Naa15 from Naa10 KO mouse tissues
514 followed by mass spectrometry analysis (Table 2) and Nt-acetylation assays (Fig 3C) fully
515 support that the endogenous Naa12-Naa15 complexes produces NatA activity. Finally, we
516 found genetic proof of the compensatory activity of Naa12 in mice when we observed
517 embryonic lethality in in *Naa10*; *Naa12* DKO male and *Naa10*$^{+/-}$; *Naa12*$^{-/-}$ female mice (Fig
518 6 and S7 Fig). This compensation by Naa12 explains the mouse proteomics data indicating
519 normal Nt-acetylation in Naa10 KO mice (Fig 3A). We have confirmed the expression of
520 Naa12 in various tissues using qPCR and Western blot analyses (S5A-S5E Fig). The band for
521 Naa12 runs a little higher in the Western blot than the calculated molecular weight would
522 suggest, which is consistent with previous observations of NAA10 gel migration. Future
523 characterization of Naa12 may define possible post-translational modifications specific for
524 Naa12 that might account for the variability of detection by the antibody.

525 Gene duplication has long been believed to be a major driving force in evolution that
526 provides genetic novelty in organisms. Paralogous genes, originating by small-scale or
527 whole-genome duplication, overlap functional roles for each other and can completely or
528 partially compensate for the loss of the duplicate gene (56, 57). There is not yet any human
529 reported with complete knockout for *NAA10*. There is one published truncating variant in the
530 C-terminal portion of NAA10 in a male patient with microphthalmia (35), but unfortunately
531 there are no cell lines available from this family to confirm whether any truncated NAA10
532 protein is expressed, as was shown with a splice-site mutation in a Lenz microphthalmia
533 family (29). NAA10 was also identified in screens for essential genes in human cell lines (58,
534 59), so it seems unlikely that an unknown NAA10-like paralogous gene exists in humans,
535 other than the already known NAA11.

536 The pleiotropic phenotypes shown in *Naa10* KO mice, including hypopigmentation
537 and supernumerary ribs with a penetrance of 100%, were not observed in the *Naa12* KO
538 mice. Naa10 itself has been described to have N-ε-acetyl-activity towards internal lysine
539 residues of proteins involved in various disease- and development-related signaling pathways
540 (11), although its acetylation of some substrates is controversial (60, 61). Since the Nt-
541 acetylome appears to be globally intact in MEFs from *Naa10* KO mice, it is possible that the
542 presented phenotypes could be due to the loss of Naa10-specific N-ε-acetyl-activity or non-
543 catalytic roles of Naa10 (4). Alternatively, the quantitative expression of Naa10 and Naa12
544 might be different within or between tissues, which might then explain why there is clearly a
545 phenotype for *Naa10*$^{+/-}$; *Naa12*$^{+/-}$ female mice (not born at Mendelian ratios and the few that
546 are born are usually much smaller) but no apparent phenotype in *Naa10*$^{+/+}$; *Naa12*$^{-/-}$ female
547 mice. It seems likely that the mechanism cannot be simply additive between two equally
548 expressed proteins, because if the expression of each protein is theoretically set at an arbitrary
549 unit of 10, then *Naa10*$^{+/-}$; *Naa12*$^{+/-}$ female mice might possibly have half as much of each
550 protein, so that the total dose of both proteins together would be 10, instead of 20. Likewise,
551 the total dose of both proteins together would also be predicted to be 10 in a *Naa10*$^{+/+}$;
552 *Naa12*$^{-/-}$ female. Yet, the *Naa10*$^{+/-}$; *Naa12*$^{+/-}$ female mice have a phenotype, whereas the
553 *Naa10*$^{+/+}$; *Naa12*$^{-/-}$ female mice do not (Fig 6). Therefore, other explanations could include
554 different tissue-specific dosages of each protein, different expression between different
555 tissues, possible X-chromosome skewing for the X-linked *Naa10* in different tissues, or

556 different functions of the two enzymes, including Naa10-specific N-ε-acetyl-activity or non-
557 catalytic roles of Naa10 (4). These questions remain unanswered and are worth exploring in
558 future studies.

559 There are several clinical features that were presented in the original description of
560 OS (26) which can now be better understood in light of the phenotypes found in the knockout
561 mouse model. For example, all of the affected children in the first families with OS were
562 noted to have large and, in some cases, persistently open fontanels (25, 26). For one child
563 (Family 1, Individual II-1), CT scanning revealed cerebral atrophy with enlarged ventricles,
564 and in another child (Family 1, Individual III-4), there was evidence on magnetic resonance
565 imaging (MRI) of "moderate lateral and third ventricular dilatation without identified cause".
566 Lastly, all of the children had respiratory depression and apneic episodes, along with varying
567 course of hypotonia and/or hypertonia (including documented hyperreflexia in at least one
568 case (Family 2, Individual III-2)). In retrospect, it seems that these clinical features could be
569 consistent with mild hydrocephaly in these probands with Ogden syndrome, which resolved
570 over time. This is also consistent with the ventriculomegaly reported in several female OS
571 probands with missense mutations in *NAA10*, along with ventriculomegaly in one other male
572 proband who died in the first week of life, with generalized hypotonia and lack of
573 spontaneous respirations (62). One of the female patients with an Arg83Cys mutation in
574 Naa10 (#9 in table 1 of that paper) was reported as having intraventricular hemorrhage in the
575 occipital horn, hypoxic-ischemic encephalopathy, and a ventriculo-peritoneal shunt. It is
576 possible that this sequence of events is compatible with hydrocephaly with clinical signs and
577 symptoms that required the placement of the shunt.

578 There are additional cardiac and skeletal features that are also worth re-examining in
579 light of these new findings. In some of the original cases of OS, there were varying levels of
580 pulmonary valve stenosis detected on echocardiography, along with some documentation of
581 pulmonary hypoplasia (26). For example, individual III-7 in Family 1 was found on
582 echocardiography to have small persistent ductus arteriosus, a mildly decreased left
583 ventricular systolic function, an abnormal appearing aortic valve, an enlargement of the right
584 ventricle, decreased right ventricular systolic function, and persistence of the foramen ovale.
585 Individual III-6 from this same extended family was found on echocardiography to have a
586 thickened bicuspid aortic valve and mild pulmonary hypertension. One of the OS female
587 patients with an Arg83Cys mutation in *NAA10* was reported to have “supernumerary
588 vertebrae” (62). Prompted by our findings of supernumerary ribs in the mice, we obtained an
589 MRI report for this patient, in which the radiologist concluded that there appeared to be 25
590 distinct vertebrae, as opposed to the usual 24, with a suggestion of a 13th rib, at least on the
591 right. The report went on to state that "the vertebrae represent 7 cervical vertebrae, 13 rib-
592 bearing thoracic vertebrae, and 5 lumbar vertebrae, and the L1 vertebra is mildly dysmorphic,
593 with a suggestion of anterior beaking". In addition, chest and abdominal X-rays from two of
594 the brothers in generation VI of a family with microphthalmia demonstrated the presence of
595 13 rib-bearing thoracic vertebrae, alongside the dramatic scoliosis in both individuals. Four
596 other females carrying mutations in Naa10 were reported as having either pectus carinatum or
597 excavatum (62), one of the boys with OS (Family 1, Individual III-4) was noted to have
598 pectus excavatum, and retrospective review of some of the clinical photographs appears to
599 show mild pectus excavatum in individual III-6 of the same family. Studies of human
600 populations have shown that the levels of transition may be shifted cephalad, resulting in 23
601 mobile vertebrae, or shifted caudad, resulting in 25 presacral vertebrae. Such variations may
602 occur in 2-11% of the population (63). In addition, the number of ribs can also vary in mice,
603 as a result of teratogenic and genetic influences (64, 65). However, the complete penetrance

604 for supernumerary ribs in the *Naa10*-deficient mice, along with the presence of extras ribs in
605 some of the patients, suggest that there is a pathway common to humans and mice that is
606 altered by mutations involving *NAA10*.

607 Several mouse mutants show similar cardiac or skeletal phenotypes to the *Naa10*-
608 deficient mice. *Pax3* mutants phenocopy our *Naa10*$^{-/-}$ mutants, as *Pax3*$^{+/-}$ adults exhibit 100%
609 piebaldism, and exhibit neural crest (NC)-related PTA/DORV with concomitant VSDs (66-
610 69). *Pax3* systemic nulls also have skeletal defects due to abnormal somite morphogenesis
611 (70, 71). Moreover, *Pax3* cKOs demonstrated that NC-specific deletion is sufficient to cause
612 DORV/VSDs and death at birth (69, 72), and that restricted deletion within the
613 neuroepithelium causes congenital hydrocephalus (73). While *Pax7* systemic deletion does
614 not cause NC-associated defects, it does exhibit overlapping expression, and Pax3-Pax7
615 compound heterozygous mice develop hydrocephalus (73), suggesting combinatorial
616 function. *Hox C8*$^{-/-}$ mice exhibit an extra rib and an extra rib articulating with the sternum
617 (74, 75), and an unfused sacral vertebra which lead to 27 presacral vertebrae (76), as seen in
618 our model. *Hox A4*$^{-/-}$ mice described in Horan et al. (77) shows cervical fusions of C2/C3, a
619 rib on C7 not fully penetrant and sternal defects with bone ossification anomalies. *Hox A5*$^{-/-}$
620 mice display numerous cervico-thoracic defects such as a rib process coming from the 7th
621 cervical vertebra, an increased in the number of sternebrae and total number of ribs (78).
622 Both *Hox A4*$^{-/-}$ and *A5*$^{-/-}$ mice exhibit an extra rib articulating with the sternum. *Hox D3*$^{-/-}$
623 mice are the only Hox gene mutation leading to cervical fusion of both the atlas and axis (79).
624 *Hox A9*$^{-/-}$ mice have anteriorization of both sacral and lumbar parts, with an extra pair of ribs
625 at the lumbar level. *Hox A9*$^{-/-}$ mice do not have any relevant sternal defect (80). *Hox B9*$^{-/-}$
626 mice have an extra rib articulating with the sternum and 14 pairs of rib (81). These
627 phenotypes, especially *Hox C8*, share common features with the *Naa10*-deficient mice. This
628 phenotype is also close to the *Rpl38* -/- phenotype (82), except for the sacral fusion described
629 in *Rpl38* -/- mice. Interestingly, it was shown that *Hox* genes were dysregulated in this
630 genotype. The skeletal findings and comparison to other mutant mice suggest a pattern
631 consistent with a homeotic anterior transformation hypothesis.

632 The developmental role of Naa10 in mice has been previously described (42). Lee *et*
633 *al.* reported embryonic lethality at E12.5-14.5 and beyond (due to placental defects),
634 hydrocephaly, postnatal growth retardation, and maternal effect lethality in *Naa10* KO mice
635 and suggested that genomic imprinting dysregulation is associated with those developmental
636 phenotypes. In the present study, hydrocephaly and postnatal growth retardation were also
637 apparent, but embryonic lethality was not observed, which prompted the search for and
638 discovery of Naa12. The previous paper (42) did not report the piebaldism, homeotic anterior
639 transformation, hydronephrosis, and genital defects (such as seminal vesicle malformation
640 and hydrometrocolpos), nor did they explain the cause of death in the first day of life, which
641 is at least partly due to congenital heart defects, as reported herein. A more recent paper from
642 the same group reported that conventional and adipose-specific Naa10p deletions in mice
643 resulted in increased energy expenditure, thermogenesis, and beige adipocyte differentiation
644 in the surviving mice (83). Although the Lee *et al.* paper reported a very high maternal effect
645 lethality rate of 90% (46/51) (otherwise stated as a survival rate of 10% (5/51)) for newborns
646 in matings following *Naa10*$^{-/-}$ female and C57BL/6J wild type male intercrossing, this rate
647 was only 29% (37/127) in this same mating herein in the first 24 hours of life and with a total
648 death rate in the first three days for all newborns of 46/127, or 36% (Table S4), with this
649 result deriving from a larger number of mating pairs, litters and pups. Although this rate of
650 36% is higher than that seen with matings involving *Naa10*$^{+/-}$ females (15.8% and 13.6%)
651 (Table S4), the explanation for this ~20% difference in survival in the first 3 days of life

652 could involve differences in maternal care provided by the *Naa10*$^{+/-}$ and *Naa10*$^{-/-}$ females, but
653 this would have to be investigated in future studies, involving detailed behavioral and
654 cognitive assessment of the dams.

655 The reasons for the differences between the studies in regards to maternal effect
656 lethality and *in utero* lethality are unknown at present. Whilst Lee *et al.* deleted *Naa10* exons
657 2-6 (42), the current study deleted *Naa10* exons 1-4 or used an allele *Naa10*^{tm1a} expressing β-
658 galactosidase instead of the *Naa10* gene (S1 Fig.), and there was not any significant
659 embryonic lethality in either line (S1 and S2 Table). All three of these mouse models were
660 made using 129Sv/Ev ES cells, and all three are nulls lacking Naa10 protein. It is the case
661 that the previous study used the Cre/loxP system to generate the *Naa10* KO mice, where a
662 floxed Naa10 female mouse was crossed with the Ella-Cre transgenic male mouse expressing
663 Cre recombinase for germ line deletion of loxP-flanked *Naa10*, whereas our mice were made
664 using standard gene-targeting methods without the use of Cre recombinase, but it is not clear
665 how this would have resulted in embryonic lethality, particularly as these mice were only
666 used after "at least six generations of backcross with C57BL/6 mice". The explanation for
667 differences in embryonic lethality might be more likely due to different combinations of
668 modifying alleles that are present in the different C57BL/6J genetic backgrounds, rather than
669 differences in our model systems, and future plans will address this after back-crossing more
670 than 20 generations to C57BL/6J to achieve an entirely inbred line. The impact of genetic
671 background is supported by the observation that additional null alleles on mixed genetic
672 backgrounds, made during the process of generating missense mouse models for OS, have far
673 less penetrance for a range of the various phenotypes, including much less perinatal lethality
674 (unpublished observations).

675 In conclusion, our study provides strong evidence that Naa10, the catalytic subunit of
676 N-acetyltransferase A (NatA), is critical for normal development in mice. Furthermore, this
677 study explains the puzzle regarding the lack of complete embryonic lethality in the *Naa10*
678 knockout mice due to the discovery of a second mouse *Naa10* paralog, which, unlike *Naa11*,
679 is expressed in the heart as well as other tissues. Taken together, our findings suggest that the
680 newly identified Naa12 can functionally rescue Naa10 loss and act as a catalytic subunit in
681 mouse NatA complexes.
682

683 ## Materials and Methods

684 **Mice.** All experiments were performed in accordance with guidelines of International Animal
685 Care and Use Committee (IACUC) of Ewha Womans University, Cold Spring Harbor
686 Laboratory, and Institute for Basic Research in Developmental Disabilities (IBR).

687

688 **Generation of *Naa10* deficient mice.** The *Naa10* knockout (KO) mice were generated as
689 previously described (39). *Naa10*^{tm1a} [B6;129P2-Ard1$^{tm1a(Eucomm)Gto}$/J] (*Naa10*^{tm1a}) mice, used
690 for *Naa10* reporter mouse, were generated using standard method based on a standard gene-
691 targeting in E14 embryonic stem (ES) cells (129/Sv) by using a targeting vector from
692 EUCOMM. Correctly targeted ES clones were used for blastocyst microinjection and
693 generation of chimeric mice. Chimeric mice were crossed to C57BL/6J mice, and then the
694 progeny were backcrossed to C57BL/6J for more than ten generations. The *Naa10*-deficient
695 mice used in the weight analyses were derived from mice backcrossed 8 times to a C57BL/6J
696 inbred genetic background, and this was confirmed with genome scanning at the Jackson
697 Laboratory, showing heterozygosity for only one marker for 129S1/SvImJ out of 290

698 autosomal markers tested, thus giving a percentage of C57BL/6J of 99.66%.
699
700 **Generation of *Naa12* knockout mice.** The mice were made using standard methods by
701 microinjection of CRISPR reagent mix into zygotes obtained from the mating of B6D2F1
702 females (i.e. 50% C57BL/6J, 50% DBA/2J (D2)) females to inbred C57BL/6J males. The
703 guide RNA was produced and validated from Sigma using a Cel1-nuclease assay, and the
704 most active guide was selected, which was Naa12_0_125 (C9587), with a target sequence of:
705 GAGCGTTTCACAGCCAGCG and including the targeting cr-RNA sequence and the
706 tracrRNA portion. The indels were transmitted by breeding again to inbred C57BL/6J males,
707 and the resulting progeny were interbred on a mixed genetic background of approximately
708 12.5% DBA/2J (D2) / 87.5% C57BL/6J, for use in the reported experiments, including the
709 weight analyses. Progeny from these mice have been backcrossed to C57BL/6J for more than
710 ten generations, with no discernible new phenotypes emerging. Genomic DNA was isolated
711 from paw and tail. DNA was screened for mutations using PCR and Surveyor assay (84),
712 followed by Sanger sequencing of selected clones and the use of CRISP-ID (85) to identify
713 putative deletions.
714
715 **Primers for mice genotyping.** The primers used for *Naa10 KO* and *Naa10*^{tm1a} genotyping
716 were Naa10-F: 5'-cctcacgtaatgctctgcaa-3', Naa10-neo-F: 5'-acgcgtcaccttaat-atgcg-3', Naa10-
717 R: 5'- tgaaagttgagggtgttgga-3', Naa10^{tm1a}-F: 5'-gcacactctctgaattggac-3', Naa10^{tm1a}-neo-F: 5'-
718 ggccgcttttctggattcat-3' and Naa10^{tm1a}-R: 5'-gcaggggaataaggcattgg-3'. The primers used for
719 Naa12 KO were Naa12 Surveyor F: 5'-gctccacctcgctaacctgg-3', Naa12 Surveyor R: 5'-
720 gccagatgacctgatgaacatgc-3' and HEX-Naa12 Surveyor F: 5'-gctccacctcgctaacctgg-3'.
721
722 **Antibodies.** The following antibodies were used: Rabbit anti-Naa10 (Abcam #ab155687),
723 rabbit anti-Naa10 (Protein Tech #14803-1-AP), rabbit monoclonal anti-NAA10
724 (CellSignaling, #13357), goat anti-Naa10 (Santa Cruz, #sc-33256), rabbit anti-Naa10 (Santa
725 Cruz, #sc-33820), rabbit anti-Naa11 (Novus Biologicals ; #NBP1-90853), mouse anti-
726 Naa15/NARG1 (Abcam ; #ab60065), rabbit polyclonal anti-NAA15 (12), rabbit anti-
727 Naa50 (LifeSpan BioSciences ; #LS-C81324-100), rabbit anti-FLAG (Sigma; #F7425),
728 mouse anti-GAPDH (Abcam ; #ab9484), goat anti-Actin (Santa Cruz, #1615), mouse anti-
729 GST (GenScript ; #A00865) and mouse anti-V5 (Life Technologies ; #R960-25). The
730 antibody against the potential mNaa10 paralog mNaa12 (Gm16286, UniProt: Q9CQX6) was
731 raised in rabbits after immunization with a synthetic peptide of the Naa12 C-terminus (aa191-
732 205: QENLAGGDSGSDGKD-C) by PrimmBiotech.
733
734 **Alcian blue and Alizarin red co-staining of skeletons.** After the skin and internal organs
735 were removed, embryos were fixed in 95% ethanol (EtOH) for 4h, then in 100% acetone for
736 overnight. Embryos were stained with 0.03% Alcian Blue 8GX in ethanol/ acetic acid (4:1
737 v/v) for overnight and kept in 1% KOH for 2 days until they became clearly visible, followed
738 by staining with 0.05% Alizarin Red in 1% KOH for 4h. After washing with 100% Glycerol/
739 1% KOH (1:1 v/v), skeletons were kept in 100% Glycerol.
740 **Isolation and imaging of mouse embryos.** Timed mating were performed either by using
741 the presence of a vaginal plug to assess fertilization. The morning vaginal plug was
742 designated E0.5. Pregnant mice were sacrificed at several time points after conception. The
743 embryos were isolated in ice-cold PBS with 1% FBS and washed three times in ice-cold PBS.
744 Embryos were imaged using a Zeiss Axiozoom V16 with Zen software and merged 50 slides
745 between Z-stack intervals.
746

β-galactosidase staining. Isolated E10.5 embryos were incubated in fixation solution (4% paraformaldehyde) at 4°C for 25min. Samples were washed in ice-cold PBS and then incubated in permeabilization solution (PBS containing 0.01% Na deoxycholate, 0.02% Nonidet-P40, 2 mM MgCl2) for 20 min at 4°C. Subsequently, samples were incubated in β-gal staining solution (PBS containing 1 mg/mL X-Gal, 5 mM potassium ferrocyanide, 5 mM potassium ferricyanide, 0.02% Nonidet-P40, 2 mM MgCl2) at 37°C overnight. Following β-gal staining, samples were washed with PBS and incubated in fixation solution at 4°C for storage.

Hematoxylin and Eosin Staining. Isolated kidney tissues at E18.5 and P3 were fixed with 4% paraformaldehyde at 4°C for overnight and embedded in paraffin. Samples were sectioned at 8 micron thick and stained with Hematoxylin (MHS80, Sigma) and Eosin (HT110116, Sigma) for morphology.

Cloning. Full-length mouse Naa10 and Naa12 expression vectors were separately constructed using a pMAL-c5x vector. In both cases, the catalytic subunit contained an N-terminal uncleavable MBP-tag. Bacterial expression vectors of mNATs were cloned from cDNA generated from mouse liver or testes. mRNA was isolated using the Oligotex direct mRNA kit (Qiagen) according to the manufacturer recommendations. 1µg RNA was reverse transcribed with Superscript IV reverse transcriptase (Thermo Fisher) and Oligo dT(18) primer. The PCR product was digested and cloned into BamHI restriction sites of pGEX-4T1 (GE Healthcare), pMAL-p5X and p3xFLAG-CMV10 (Sigma-Aldrich) using standard techniques. All constructs were sequenced to validate correct insert and orientation.

Primers for cloning. cDNA was amplified using the primers CCG GGA TCC ATG AAC ATC CGC AAT and CTG GGA TCC CTA GGA GGC AGA GTC AGA for mNaa10 variants, CCG GGA TCC ATG AAC ATC CGC AAT GC and CTG GGA TCC CTA GGA GAT GGA ATC CAA GTC for mNaa11, CCG GGA TCC ATG AAC ATC CGC CGG and CTG GGA TCC CTA GGA GGC GGA CCC TAG for mNaa12.

Peptide competition assay. To determine the specificity of the mNaa12 antibody, a peptide competition assay was performed using the same peptide as used for immunization (aa 191-205: QENLAGGDSGSDGKD-C). 100 µg antibody were bound to 50 mg peptide-coupled CNBr-sepharose (10 mg peptide/g sepharose) in PBS + 0.2 % Triton X-100 for 1 h at 4° C on an orbital shaker. The beads were pelleted by centrifugation at 2.700 × g for 3 min at 4°C and 250 µl of the antibody-depleted supernatant diluted in 5 mL TST for detection (1:100 final antibody dilution). Western blots of mouse lysates were probed with the depleted antibody or untreated antibody as control (1:100 dilution in TST).

Co-immunoprecipitation assay. Protein-protein interaction studies were performed in HEK293 cells. Briefly, 8 x 10^5 cells were seeded per well in 6-well plates. After 24 h, cells were co-transfected with pcDNA3.1/V5-His-mNaa15 and p3xFLAG-CMV10-Naa10^{235} (isoform 1), -Naa10^{225} (isoform 2), -Naa11 or -Naa12 or the corresponding empty vectors. Cells were lysed after 48 h in 200 µl PBS-X per well and cellular debris pelleted at 20.800×g for 10 min at 4°C. 350 µl of the generated lysate was incubated with 1 µg anti-V5 antibody for 1 h at 4°C, followed by a 30 min incubation with 30 µl protein-A sepharose (Sigma-Aldrich). Protein complexes were washed three times by centrifugation (2.700×g, 2 min) and eluted in 30 µl 2×SDS sample buffer.

795 Proteins were separated by SDS-PAGE and transferred onto a nitrocellulose membrane
796 (Amersham Protran 0.2 µM NC) by immunoblotting. The membrane was blocked in 5% non-
797 fat dry milk and incubated overnight with rabbit polyclonal anti-NAA15(12) (1:2000,
798 BioGenes) and rabbit monoclonal anti-NAA10 (anti-ARD1A, 1:1000, CellSignaling,
799 #13357) diluted in 1xPBS containing 1% non-fat dry milk and 0.1% Tween. The
800 immunoblots were washed and incubated for 1 h at RT with HRP-linked secondary antibody
801 donkey anti-rabbit IgG (GE Healthcare, NA934). The HRP-signal was detected using
802 SuperSignalTM West Pico PLUS Chemiluminescent Substrate Kit (Thermo Scientific) and
803 ChemiDocTM XRS+ system (Bio-Rad) and visualised by ImagelabTM Software (Bio-Rad).
804
805 **Immunoprecipitation of Naa15 to form NatA complex.** For immunoprecipitation of
806 Naa15, 90-120 mg liver tissue from a WT- and Naa10 KO mouse was lysed in 500 µl IPH
807 lysis buffer (50 mM Tris-HCl pH 8.0, 150 mM NaCl, 5 mM EDTA, 0.5% NP-40, 1×
808 complete EDTA-free protease inhibitor cocktail (Roche) using Kontes Pellet Pestle Motor
809 and incubated on ice for 40 min. Cell debris was pelleted by centrifugation (17000 × *g*, 4 °C,
810 10 min) and the supernatants transferred to new eppendorf tubes. The protein concentration
811 was determined by BCA Protein Assay Kit (Thermo Scientific) and the tissue lysates were
812 subsequently diluted with IPH lysis buffer to an equal protein concentration of 25 µg/µl. The
813 WT- and Naa10 KO tissue lysates were then divided in two, whereof one half was mixed with
814 15 µg of anti-Naa15 antibody and the other half with 15 µg of anti-V5 antibody as a negative
815 control. The mixtures were incubated at 4 °C for 3 h on a rotator. Afterwards, 180 µl of
816 Protein A/G magnetic beads (Millipore) pre-washed in IPH lysis buffer was added to each
817 sample and incubated overnight. Then, the magnetic beads were washed three times in IPH
818 lysis buffer and two times in 1x acetylation buffer (100 mM Tris-HCl pH 8.5, 2 mM EDTA,
819 20% Glycerol) prior to being resuspended in 90 µl of 2x Acetylation buffer and used in a
820 [^{14}C]-Ac-CoA–Based acetylation assay.
821
822 **[^{14}C]-Ac-CoA–based acetylation assay of immunoprecipitated samples.** Three positive
823 replicates were prepared for each IP sample containing 10 µl IP beads, 200 µM synthetic
824 oligopeptide $SESS_{24}$ (BioGenes), 100 µM [^{14}C]-Ac-CoA (Perkin-Elmer) and dH_2O to a final
825 volume of 25 µl. In addition, two replicates for each IP sample were prepared without
826 synthetic oligopeptide as negative controls. The samples were incubated at 37 °C for 45 min
827 in a thermomixer with shaking at 1400 rpm. Finally, the magnetic beads were isolated and 23
828 µl of the supernatant transferred to P81 phosphocellulose filter discs (Millipore). The filter
829 discs were washed three times for 5 min in 10 mM HEPES buffer (pH 7.4) and air dried. To
830 determine the amount of incorporated [^{14}C]-Ac, the filter discs were added to 5 mL Ultima
831 Gold F scintillation mixture (Perkin-Elmer) and analysed by a Perkin-Elmer TriCarb 2900TR
832 Liquid Scintillation Analyzer.
833
834 **Proteomics sample preparation.** Immunoprecipitation of Naa15 from a WT- and Naa10 KO
835 mouse was performed as described above. Bound proteins were eluted from the magnetic
836 beads using 60 µl of elution buffer (2% SDS, 100 mM Tris-HCl pH 7.6, 0.1 M DTT) and
837 heated for 5 min at 95 °C. The eluates were processed for LC-MS/MS analysis using filter-
838 aided sample preparation (FASP) method(86). The eluted protein mixtures were mixed with
839 UA buffer (8 M urea, 100 Mm Tris-HCl pH 8.0) and centrifuged through Microcon 30kDa
840 MWCO filters followed by Cys-alkylation with 50 mM iodoacetamide dissolved in UA
841 buffer. Afterwards, the buffer was exchanged with 50 mM ammonium bicarbonate through
842 sequential centrifugation, proteins were trypsinized (Sequencing Grade Modified Trypsin,

843 Promega) and digested peptides were collected by centrifugation. Peptides were acidified
844 using 5% formic acid and desalted using C18-stagetips according to protocol(87). Briefly, 40
845 µg peptides from each sample were loaded onto C18-stagetips pre-conditioned with buffer A
846 (1% formic acid). The C18-stagetips were then washed with buffer A, before peptides were
847 eluted with buffer B (80% acetonitrile/ACN, 1% formic acid). The final eluate was
848 concentrated by Speedvac to evaporate ACN and diluted to desired volume with 5% formic
849 acid.
850
851 **Mass spectrometric analysis**. 1 µg of the peptide samples were injected into an Ultimate
852 3000 RSLC system (Thermo Scientific) connected to a Q-Exactive HF mass spectrometer
853 (Thermo Scientific) equipped with EASY-spray nano-electrospray ion source (Thermo
854 Scientific). Trapping and desalting was performed with 0.1% TFA (flow rate 5 µl/min, 5 min)
855 on a pre-column (Acclaim PepMap 100, 2 cm x 75 µm ID nanoViper column, 3 µm C18
856 beads). Peptides were separated on an analytical column (PepMap RSLC, 50cm x 75 µm i.d.
857 EASY-spray column, 2 µm C18 beads) during a biphasic ACN gradient with a flow rate of
858 200 nl/min. Solvent A (0.1% FA (vol/vol) in water) and B (100% ACN) were used for the
859 following gradient composition: 5% B for 5 min, 5-8% B for 0.5 min, 8–24% B for 109.5
860 min, 24–35% B for 25 min and 35–80% B for 15 min, 80% B for 15 min and conditioning
861 with 5% B for 20 min. The mass spectrometer was operated in data-dependent mode to
862 automatically switch between full scan MS and MS/MS acquisition. MS spectra (m/z 375-
863 1500) were acquired with a resolution of 120 000 at m/z 200, automatic gain control (AGC)
864 target of 3 x 106 and maximum injection time (IT) of 100 ms. The 12 most intense peptides
865 above an intensity threshold (50 000 counts, charge states 2-5) were sequentially isolated to
866 an AGC target of 1 x 105 and maximum IT of 100 ms and isolation width maintained at 1.6
867 m/z, before fragmentation at a normalised collision energy of 28%. Fragments were detected
868 in the orbitrap at a resolution of 15 000 at m/z 200, with first mass fixed at m/z 100. Dynamic
869 exclusion was utilized with an exclusion time of 25 s and "exclude isotopes" enabled. Lock-
870 mass internal calibration (m/z 445.12003) was used. Raw files were processed with
871 MaxQuant v. 1.5.5.1(88) and searched against a database of Swiss-Prot annotated mouse
872 protein sequences (retrieved 22.06.2018) in which the Naa12 sequence was added manually,
873 and with a reverse decoy database. MaxQuant was run with default settings. Peptide and
874 protein identifications were filtered to a 1 % false discovery rate (FDR). Minimum peptide
875 length was set to 7. Modifications included in protein quantification were oxidation (M), Nt-
876 acetylation, lysine acetylation, tryptophan hydroxylation and phosphorylation (STY). Other
877 parameters: match between runs – true, matching time window – 0.7 min, alignment time
878 window – 20 min, find dependent peptides – true, mass bin size – 0.0065.
879
880 **Whole body CT scanning.** CT scans were acquired on a Nanoscan PET/CT scanner from
881 Mediso using Nucline v2.01 software. All mice were kept sedated under isoflurane anesthesia
882 for the duration of the scan. Scans were acquired with an X-ray tube energy and current of
883 70kVp and 280uA respectively. 720 projections were acquired per rotation, for 3 rotations,
884 with a scan time of approximately 11 minutes, followed by reconstruction with a RamLak
885 filter and voxel size 40x40x122µm. For *ex vivo* analyses, mouse heads were fixed in 10%
886 formalin buffered saline, followed by scanning and reconstruction with 1440 projections per
887 revolution. Cranial volume was measured using VivoQuant software (v2.50patch2), using
888 the spline tool to manually and accurately draw around the circumference of the cranium on
889 multiple stepwise 2D slices.
890
891 **Integrated N-terminal peptide enrichment (iNrich) assay.** iNrich assays were performed

892 as described(43). Mouse embryonic fibroblasts (MEFs) were made from E13.5 embryos,
893 using standard techniques, with DMEM media supplemented with 10% fetal bovine serum
894 (FBS), L-glutamine and penicillin/streptomycin. Cells were harvested by trypsinization,
895 washed twice with ice-cold PBS (phosphate-buffered saline, pH 7.4; Gibco), and resuspended
896 in ice-cold lysis buffer containing 0.2 M EPPS (pH 8.0), 6 M guanidine, 10 mM TCEP
897 (Thermo Fisher Scientific), and 40 mM 2-chloroacetamide (Sigma-Aldrich). After 10 min of
898 incubation on 95 °C, cells were lysed by ultrasonication by a BranSonic 400B. The proteins
899 from the cell lysate were isolated by transferring supernatant after centrifugation at 12000g
900 for 10 min at 4 °C. The protein concentration of the collected supernatant was determined by
901 BCA (bicinchoninic acid) protein assay
902
903 **RNA and protein isolation and assays.** 70-120 mg tissues were lysed in 5 µl/mg tissue RIPA
904 buffer (Sigma) with 1x Complete protease inhibitors and 1 U/µl Superase In RNase inhibitor
905 (Thermo Scientific) using Fisherbrand Pellet Pestle Cordless Motor. After homogenization
906 debris was removed by centrifugation at 20.800 g for 10 min at 4°C. Protein concentration
907 was determined using APA assay (Cytoskeleton Inc.) and 50 µg total protein were separated
908 on SDS-PAGE followed by western blot. Membranes were stained with anti-Naa10, anti-
909 Naa15 and anti-GAPDH antibodies (all Abcam).

910 For RNA purification, 30 µl clarified lysate were mixed with 70 µl RNase free water and
911 RNA isolated using the RNeasy Mini Kit (Qiagen) according the manufacturers
912 recommendations, including on-column Dnase digest. 1 µg RNA was reverse transcribed
913 using the TaqMan Reverese transcription kit and gene level detection performed using SYBR
914 Green Master Mix (all Thermo Scientific). Relative expression was normalized to GAPDH
915 and ACTB.

916 For the characterization of the mNaa12 antibody, tissue was lysed in 2 µl per mg tissue PBS-
917 X (PBS + 0.2 % (v/v) Triton X-100 + 1 × Complete protease inhibitor cocktail). 10-200 µg
918 lysate were subjected to SDS-PAGE and western blot.
919
920 **Primers for mice qPCR.** The following primers pairs were used: mNaa10-Exon2/3-F: 5'-
921 ctcttggccccagctttctt-3' and mNaa10-Exon3/4-R: 5'- tcgtctgggtcctcttccat -3', mNaa11-F: 5'-
922 accccacaagcaaagacagtg-3' and mNaa11-R: 5'- agcgatgctcaggaaatgctct -3',
923 mNaa12(Gm16286)-F: 5'-acgcgtatgctatgaagcga-3' and mNaa12(Gm16286)-R: 5'-
924 ccaggaagtgtgctaccctg-3', mNaa15-F: 5'-gcagagcatggagaaaccct-3' and mNaa15-R: 5'-
925 tctcaaacctctgcgaacca-3', mNaa50-F: 5'-taggatgccttgcaccttacc-3' and mNaa50-R: 5'-
926 gtcaatcgctgactcattgct-3', mGAPDH-F: 5'-aggtcggtgtgaacggatttg-3' and mGAPDH-R: 5'-
927 tgtagaccatgtagttgaggtca-3', mACTB-F: 5'-ggctgtattcccctccatcg-3' and mACTB-R: 5'-
928 ccagttggtaacaatgccatgt-3'.
929
930 **Expression and purification of WT mouse, Naa10 and Naa12.** All constructs were
931 expressed in Rosetta (DE3)pLysS competent *E. coli* cells. Cells were grown in LB-media to
932 OD_{600} 0.6-0.7 prior to inducing protein expression with 0.5 mM isopropyl β-D-1-
933 thiogalactopyranoside (IPTG) at 18°C for ~16 hrs. All subsequent purification steps were
934 carried out at 4°C. Cells were isolated by centrifugation and lysed in lysis buffer containing
935 25 mM Tris, pH 8.0, 150 mM NaCl, 10 mM β-mercaptoethanol (β-ME), 10 µg/mL
936 phenylmethanesulfonylfluoride (PMSF), and DNase. The lysate was clarified by
937 centrifugation and incubated with amylose agarose resin (New England Biolabs) for 1 hour
938 before washing the resin with ≥100 column volumes of lysis buffer and then eluted with ten
939 column volumes of lysis buffer supplemented with 20 mM maltose. The resulting eluent was

940 pooled and concentrated to ~10 mg/mL (30 kDa concentrator; Amicon Ultra, Millipore) such
941 that 500 µl was loaded onto on a Superdex 200 Increase 10/300 GL gel filtration column (GE
942 Healthcare). The gel filtration run was performed in sizing buffer containing 25 mM HEPES,
943 pH 7.0, 200 mM NaCl, and 1 mM TCEP. Peak fractions running at ~14 mL were pooled,
944 concentrated to 0.6 (6.1 µM) WT mouse Naa10 and 0.3 mg/mL (3.5 µM) WT mouse Naa12,
945 as measured by UV_{280} (Nanodrop 2000; Thermo Fisher Scientific), and stored at 4°C.
946
947 ***In vitro* radioactive acetyltransferase assays.** The assays were carried out in 40 mM
948 HEPES, pH 7.5 200 mM NaCl, where reactions were incubated with 150 nM of the gel-
949 filtration purified WT mouse Naa10 or Naa12 in a 30 µl reaction volume containing each 250
950 µM substrate peptide and radiolabeled [^{14}C]acetyl-CoA (4 mCi/mmol; PerkinElmer Life
951 Sciences) for 12 min (Naa12) or 13 min (Naa10) at 25°C. Respective time points were
952 selected to ensure detection of sufficient activity within the linear range as determined by a
953 time course experiment. The substrate peptides used in the assay corresponds to the first 7
954 amino acids of β-actin (DDDIAAL-), γ-actin (EEEIAAL-), or the *in vitro* NatA complex
955 substrate High mobility group protein A1(SESSS-) , along with C-terminal positively charged
956 residues for capture to the anion exchange paper. Background control reactions were
957 performed in the absence of enzyme or in the absence of substrate peptide to ensure that any
958 possible signal due to chemical acetylation was negligible. Each reaction was performed in
959 triplicate.

960 To quench the reaction, 20 µl of the reaction mixture was added to negatively charged P81
961 phosphocellulose squares (EMD Millipore), and the paper disks were immediately placed in
962 wash buffer (10 mM HEPES, pH 7.5). The paper disks were washed three times, at 5 min per
963 wash, to remove unreacted acetyl-CoA. The papers were then dried with acetone and added
964 to 4 mL of scintillation fluid, and the signal was measured with a PerkinElmer Life Sciences
965 Tri-Carb 2810 TR liquid scintillation analyzer. The counts per minute were converted to
966 molar units using a standard curve of known [^{14}C]acetyl-CoA concentrations in scintillation
967 fluid.

968 Full peptide sequences:
969 β-actin: NH2-DDDIAALRWGRPVGRRRRPVRVYP-COOH
970 γ-actin: NH2-EEEIAALRWGRPVGRRRRPVRVYP-COOH
971 Histone H4: NH2-SGRGKGGKGLGKGGAKRHR-COOH
972
973 **Statistical analyses.** Significant differences ($p<0.05$) are indicated by asterisks. Weight
974 analyses were performed using generalized estimating equations (GEEs) (89), an extension of
975 generalized linear models which adjusts for the effects of autocorrelation resulting from
976 multiple measurements, and implemented within version 15.1 of Stata (Statacorp 2017).
977

978 ## Acknowledgments

979 G.T.O. thanks Huiju Jo for supporting mouse genotyping. G.J.L. would like to thank Ryan
980 Driscoll for mouse genotyping, Fatima Inusa for embryo dissection, Jemima Kadima for
981 mouse husbandry, Leyi Li for transgenic mouse assistance, Melissa Nashat, Jodi Coblentz,
982 Rachel Rubino, and Lisa Bianco for veterinary advice, and Vicky Brandt for editorial
983 assistance.

984 This work was supported by a National Research Foundation of Korea (NRF) grant funded
985 by the Korean Government (2020R1A3B2079811, 2017RIDIAB03032286 and

2020RICIC1007686). Research reported in this publication was also supported by the National Institute of General Medical Sciences of the National Institutes of Health (NIH) under Award Numbers R35GM133408 (G.J.L) and R35GM118090 (R.M.), and NIH grant HL148165 (S.J.C.). The content is solely the responsibility of the authors and does not necessarily represent the official views of the National Institutes of Health. Funding was also provided by the Stanley Institute for Cognitive Genomics at Cold Spring Harbor Laboratory, the George A. Jervis Clinic and the Department of Human Genetics, Laboratory of Genomic Medicine at the New York State Institute for Basic Research in Developmental Disabilities (IBR), New York State Office for People with Developmental Disabilities. The work was also supported by the Research Council of Norway (Project 249843), the Norwegian Health Authorities of Western Norway (Projects 912176 and F-12540-D11382), and the Norwegian Cancer Society. Part of the work was carried out at the Proteomics Unit at University of Bergen (PROBE).

Competing interests

The authors declare no competing interest.

References

1. Arnesen T, Van Damme P, Polevoda B, Helsens K, Evjenth R, Colaert N, et al. Proteomics analyses reveal the evolutionary conservation and divergence of N-terminal acetyltransferases from yeast and humans. Proc Natl Acad Sci U S A. 2009;106(20):8157-62.
2. Dorfel MJ, Lyon GJ. The biological functions of Naa10 - From amino-terminal acetylation to human disease. Gene. 2015;567(2):103-31.
3. Polevoda B, Arnesen T, Sherman F. A synopsis of eukaryotic Nalpha-terminal acetyltransferases: nomenclature, subunits and substrates. BMC Proc. 2009;3 Suppl 6:S2.
4. Aksnes H, Ree R, Arnesen T. Co-translational, Post-translational, and Non-catalytic Roles of N-Terminal Acetyltransferases. Mol Cell. 2019;73(6):1097-114.
5. Starheim KK, Gevaert K, Arnesen T. Protein N-terminal acetyltransferases: when the start matters. Trends Biochem Sci. 2012;37(4):152-61.
6. Ree R, Varland S, Arnesen T. Spotlight on protein N-terminal acetylation. Exp Mol Med. 2018;50(7):1-13.
7. Shemorry A, Hwang CS, Varshavsky A. Control of protein quality and stoichiometries by N-terminal acetylation and the N-end rule pathway. Mol Cell. 2013;50(4):540-51.
8. Dikiy I, Eliezer D. N-terminal acetylation stabilizes N-terminal helicity in lipid- and micelle-bound alpha-synuclein and increases its affinity for physiological membranes. J Biol Chem. 2014;289(6):3652-65.
9. Holmes WM, Mannakee BK, Gutenkunst RN, Serio TR. Loss of amino-terminal acetylation suppresses a prion phenotype by modulating global protein folding. Nat Commun. 2014;5:4383.
10. Scott DC, Monda JK, Bennett EJ, Harper JW, Schulman BA. N-terminal acetylation acts as an avidity enhancer within an interconnected multiprotein complex. Science. 2011;334(6056):674-8.
11. Lee MN, Kweon HY, Oh GT. N-alpha-acetyltransferase 10 (NAA10) in development: the role of NAA10. Exp Mol Med. 2018;50(7):87.
12. Arnesen T, Anderson D, Baldersheim C, Lanotte M, Varhaug JE, Lillehaug JR. Identification and characterization of the human ARD1-NATH protein acetyltransferase complex. Biochem J. 2005;386(Pt 3):433-43.

1033 13. Arnesen T, Starheim KK, Van Damme P, Evjenth R, Dinh H, Betts MJ, et al. The
1034 chaperone-like protein HYPK acts together with NatA in cotranslational N-terminal
1035 acetylation and prevention of Huntingtin aggregation. Mol Cell Biol. 2010;30(8):1898-909.
1036 14. Gottlieb L, Marmorstein R. Structure of Human NatA and Its Regulation by the
1037 Huntingtin Interacting Protein HYPK. Structure. 2018;26(7):925-35 e8.
1038 15. Arnesen T, Gromyko D, Pendino F, Ryningen A, Varhaug JE, Lillehaug JR. Induction
1039 of apoptosis in human cells by RNAi-mediated knockdown of hARD1 and NATH,
1040 components of the protein N-alpha-acetyltransferase complex. Oncogene. 2006;25(31):4350-
1041 60.
1042 16. Gendron RL, Laver NV, Good WV, Grossniklaus HE, Miskiewicz E, Whelan MA, et
1043 al. Loss of tubedown expression as a contributing factor in the development of age-related
1044 retinopathy. Invest Ophthalmol Vis Sci. 2010;51(10):5267-77.
1045 17. Wang Y, Mijares M, Gall MD, Turan T, Javier A, Bornemann DJ, et al. Drosophila
1046 variable nurse cells encodes arrest defective 1 (ARD1), the catalytic subunit of the major N-
1047 terminal acetyltransferase complex. Dev Dyn. 2010;239(11):2813-27.
1048 18. Chen D, Zhang J, Minnerly J, Kaul T, Riddle DL, Jia K. daf-31 encodes the catalytic
1049 subunit of N alpha-acetyltransferase that regulates Caenorhabditis elegans development,
1050 metabolism and adult lifespan. PLoS Genet. 2014;10(10):e1004699.
1051 19. Linster E, Stephan I, Bienvenut WV, Maple-Grodem J, Myklebust LM, Huber M, et
1052 al. Downregulation of N-terminal acetylation triggers ABA-mediated drought responses in
1053 Arabidopsis. Nat Commun. 2015;6:7640.
1054 20. Ree R, Myklebust LM, Thiel P, Foyn H, Fladmark KE, Arnesen T. The N-terminal
1055 acetyltransferase Naa10 is essential for zebrafish development. Biosci Rep. 2015;35(5).
1056 21. Feng J, Li R, Yu J, Ma S, Wu C, Li Y, et al. Protein N-terminal acetylation is required
1057 for embryogenesis in Arabidopsis. J Exp Bot. 2016;67(15):4779-89.
1058 22. Chen H, Li S, Li L, Wu W, Ke X, Zou W, et al. Nalpha-Acetyltransferases 10 and 15
1059 are Required for the Correct Initiation of Endosperm Cellularization in Arabidopsis. Plant
1060 Cell Physiol. 2018;59(10):2113-28.
1061 23. Mullen JR, Kayne PS, Moerschell RP, Tsunasawa S, Gribskov M, Colavito-
1062 Shepanski M, et al. Identification and characterization of genes and mutants for an N-
1063 terminal acetyltransferase from yeast. EMBO J. 1989;8(7):2067-75.
1064 24. Polevoda B, Sherman F. Composition and function of the eukaryotic N-terminal
1065 acetyltransferase subunits. Biochem Biophys Res Commun. 2003;308(1):1-11.
1066 25. Myklebust LM, Van Damme P, Stove SI, Dorfel MJ, Abboud A, Kalvik TV, et al.
1067 Biochemical and cellular analysis of Ogden syndrome reveals downstream Nt-acetylation
1068 defects. Hum Mol Genet. 2015;24(7):1956-76.
1069 26. Rope AF, Wang K, Evjenth R, Xing J, Johnston JJ, Swensen JJ, et al. Using VAAST
1070 to identify an X-linked disorder resulting in lethality in male infants due to N-terminal
1071 acetyltransferase deficiency. Am J Hum Genet. 2011;89(1):28-43.
1072 27. Van Damme P, Stove SI, Glomnes N, Gevaert K, Arnesen T. A Saccharomyces
1073 cerevisiae model reveals in vivo functional impairment of the Ogden syndrome N-terminal
1074 acetyltransferase NAA10 Ser37Pro mutant. Mol Cell Proteomics. 2014;13(8):2031-41.
1075 28. Dorfel MJ, Fang H, Crain J, Klingener M, Weiser J, Lyon GJ. Proteomic and
1076 genomic characterization of a yeast model for Ogden syndrome. Yeast. 2017;34(1):19-37.
1077 29. Esmailpour T, Riazifar H, Liu L, Donkervoort S, Huang VH, Madaan S, et al. A
1078 splice donor mutation in NAA10 results in the dysregulation of the retinoic acid signalling
1079 pathway and causes Lenz microphthalmia syndrome. J Med Genet. 2014;51(3):185-96.
1080 30. Popp B, Stove SI, Endele S, Myklebust LM, Hoyer J, Sticht H, et al. De novo
1081 missense mutations in the NAA10 gene cause severe non-syndromic developmental delay in

1082 males and females. Eur J Hum Genet. 2015;23(5):602-9.
1083 31. Casey JP, Stove SI, McGorrian C, Galvin J, Blenski M, Dunne A, et al. NAA10
1084 mutation causing a novel intellectual disability syndrome with Long QT due to N-terminal
1085 acetyltransferase impairment. Sci Rep. 2015;5:16022.
1086 32. McTiernan N, Stove SI, Aukrust I, Marli MT, Myklebust LM, Houge G, et al.
1087 NAA10 dysfunction with normal NatA-complex activity in a girl with non-syndromic ID and
1088 a de novo NAA10 p.(V111G) variant - a case report. BMC Med Genet. 2018;19(1):47.
1089 33. Ree R, Geithus AS, Torring PM, Sorensen KP, Damkjaer M, study DDD, et al. A
1090 novel NAA10 p.(R83H) variant with impaired acetyltransferase activity identified in two
1091 boys with ID and microcephaly. BMC Med Genet. 2019;20(1):101.
1092 34. Stove SI, Blenski M, Stray-Pedersen A, Wierenga KJ, Jhangiani SN, Akdemir ZC, et
1093 al. A novel NAA10 variant with impaired acetyltransferase activity causes developmental
1094 delay, intellectual disability, and hypertrophic cardiomyopathy. Eur J Hum Genet.
1095 2018;26(9):1294-305.
1096 35. Cheng H, Gottlieb L, Marchi E, Kleyner R, Bhardwaj P, Rope AF, et al. Phenotypic
1097 and biochemical analysis of an international cohort of individuals with variants in NAA10
1098 and NAA15. Hum Mol Genet. 2019;28(17):2900-19.
1099 36. Wu Y, Lyon GJ. NAA10-related syndrome. Exp Mol Med. 2018;50(7):1-10.
1100 37. Arnesen T, Betts MJ, Pendino F, Liberles DA, Anderson D, Caro J, et al.
1101 Characterization of hARD2, a processed hARD1 gene duplicate, encoding a human protein
1102 N-alpha-acetyltransferase. BMC Biochem. 2006;7:13.
1103 38. Pang AL, Clark J, Chan WY, Rennert OM. Expression of human NAA11 (ARD1B)
1104 gene is tissue-specific and is regulated by DNA methylation. Epigenetics. 2011;6(11):1391-9.
1105 39. Yoon H, Kim HL, Chun YS, Shin DH, Lee KH, Shin CS, et al. NAA10 controls
1106 osteoblast differentiation and bone formation as a feedback regulator of Runx2. Nat
1107 Commun. 2014;5:5176.
1108 40. Conway SJ, Kruzynska-Frejtag A, Kneer PL, Machnicki M, Koushik SV. What
1109 cardiovascular defect does my prenatal mouse mutant have, and why? Genesis. 2003;35(1):1-
1110 21.
1111 41. Pun A, Cervantes I, Nieto B, Salgado C, Perez-Cabal MA, Ibanez-Escriche N, et al.
1112 Genetic parameters for birthweight environmental variability in mice. J Anim Breed Genet.
1113 2013;130(5):404-14.
1114 42. Lee CC, Peng SH, Shen L, Lee CF, Du TH, Kang ML, et al. The Role of N-alpha-
1115 acetyltransferase 10 Protein in DNA Methylation and Genomic Imprinting. Mol Cell.
1116 2017;68(1):89-103 e7.
1117 43. Ju S, Kwon Y, Kim JM, Park D, Lee S, Lee JW, et al. iNrich, Rapid and Robust
1118 Method to Enrich N-Terminal Proteome in a Highly Multiplexed Platform. Anal Chem.
1119 2020;92(9):6462-9.
1120 44. Van Damme P, Hole K, Pimenta-Marques A, Helsens K, Vandekerckhove J, Martinho
1121 RG, et al. NatF contributes to an evolutionary shift in protein N-terminal acetylation and is
1122 important for normal chromosome segregation. PLoS Genet. 2011;7(7):e1002169.
1123 45. Ingram AK, Cross GA, Horn D. Genetic manipulation indicates that ARD1 is an
1124 essential N(alpha)-acetyltransferase in Trypanosoma brucei. Mol Biochem Parasitol.
1125 2000;111(2):309-17.
1126 46. Foyn H, Jones JE, Lewallen D, Narawane R, Varhaug JE, Thompson PR, et al.
1127 Design, synthesis, and kinetic characterization of protein N-terminal acetyltransferase
1128 inhibitors. ACS Chem Biol. 2013;8(6):1121-7.
1129 47. Van Damme P, Evjenth R, Foyn H, Demeyer K, De Bock PJ, Lillehaug JR, et al.
1130 Proteome-derived peptide libraries allow detailed analysis of the substrate specificities of

1131 N(alpha)-acetyltransferases and point to hNaa10p as the post-translational actin N(alpha)-
1132 acetyltransferase. Mol Cell Proteomics. 2011;10(5):M110 004580.
1133 48. Liszczak G, Goldberg JM, Foyn H, Petersson EJ, Arnesen T, Marmorstein R.
1134 Molecular basis for N-terminal acetylation by the heterodimeric NatA complex. Nat Struct
1135 Mol Biol. 2013;20(9):1098-105.
1136 49. Sugiura N, Adams SM, Corriveau RA. An evolutionarily conserved N-terminal
1137 acetyltransferase complex associated with neuronal development. J Biol Chem.
1138 2003;278(41):40113-20.
1139 50. Park EC, Szostak JW. ARD1 and NAT1 proteins form a complex that has N-terminal
1140 acetyltransferase activity. EMBO J. 1992;11(6):2087-93.
1141 51. Gautschi M, Just S, Mun A, Ross S, Rucknagel P, Dubaquie Y, et al. The yeast
1142 N(alpha)-acetyltransferase NatA is quantitatively anchored to the ribosome and interacts with
1143 nascent polypeptides. Mol Cell Biol. 2003;23(20):7403-14.
1144 52. Magin RS, Deng S, Zhang H, Cooperman B, Marmorstein R. Probing the interaction
1145 between NatA and the ribosome for co-translational protein acetylation. PLoS One.
1146 2017;12(10):e0186278.
1147 53. Varland S, Arnesen T. Investigating the functionality of a ribosome-binding mutant of
1148 NAA15 using Saccharomyces cerevisiae. BMC Res Notes. 2018;11(1):404.
1149 54. Kim SH, Park JA, Kim JH, Lee JW, Seo JH, Jung BK, et al. Characterization of
1150 ARD1 variants in mammalian cells. Biochem Biophys Res Commun. 2006;340(2):422-7.
1151 55. Singh P, Schimenti JC, Bolcun-Filas E. A mouse geneticist's practical guide to
1152 CRISPR applications. Genetics. 2015;199(1):1-15.
1153 56. Peng J. Gene redundancy and gene compensation: An updated view. J Genet
1154 Genomics. 2019;46(7):329-33.
1155 57. Veitia RA. Gene Duplicates: Agents of Robustness or Fragility? Trends Genet.
1156 2017;33(6):377-9.
1157 58. Blomen VA, Majek P, Jae LT, Bigenzahn JW, Nieuwenhuis J, Staring J, et al. Gene
1158 essentiality and synthetic lethality in haploid human cells. Science. 2015;350(6264):1092-6.
1159 59. Wang T, Birsoy K, Hughes NW, Krupczak KM, Post Y, Wei JJ, et al. Identification
1160 and characterization of essential genes in the human genome. Science. 2015;350(6264):1096-
1161 101.
1162 60. Magin RS, March ZM, Marmorstein R. The N-terminal Acetyltransferase
1163 Naa10/ARD1 Does Not Acetylate Lysine Residues. J Biol Chem. 2016;291(10):5270-7.
1164 61. Vo TTL, Park JH, Lee EJ, Nguyen YTK, Han BW, Nguyen HTT, et al.
1165 Characterization of Lysine Acetyltransferase Activity of Recombinant Human
1166 ARD1/NAA10. Molecules. 2020;25(3).
1167 62. Saunier C, Stove SI, Popp B, Gerard B, Blenski M, AhMew N, et al. Expanding the
1168 Phenotype Associated with NAA10-Related N-Terminal Acetylation Deficiency. Hum Mutat.
1169 2016;37(8):755-64.
1170 63. Bornstein PE, Peterson RR. Numerical variation of the presacral vertebral column in
1171 three population groups in North America. Am J Phys Anthropol. 1966;25(2):139-46.
1172 64. Chernoff N, Rogers JM. Supernumerary ribs in developmental toxicity bioassays and
1173 in human populations: incidence and biological significance. J Toxicol Environ Health B Crit
1174 Rev. 2004;7(6):437-49.
1175 65. Mc LA, Michie D. Factors affecting vertebral variation in mice. 4. Experimental
1176 proof of the uterine basis of a maternal effect. J Embryol Exp Morphol. 1958;6(4):645-59.
1177 66. Conway SJ, Henderson DJ, Copp AJ. Pax3 is required for cardiac neural crest
1178 migration in the mouse: evidence from the splotch (Sp2H) mutant. Development.
1179 1997;124(2):505-14.

1180 67. Conway SJ, Henderson DJ, Kirby ML, Anderson RH, Copp AJ. Development of a
1181 lethal congenital heart defect in the splotch (Pax3) mutant mouse. Cardiovasc Res.
1182 1997;36(2):163-73.
1183 68. van den Hoff MJ, Moorman AF. Cardiac neural crest: the holy grail of cardiac
1184 abnormalities? Cardiovasc Res. 2000;47(2):212-6.
1185 69. Olaopa M, Zhou HM, Snider P, Wang J, Schwartz RJ, Moon AM, et al. Pax3 is
1186 essential for normal cardiac neural crest morphogenesis but is not required during migration
1187 nor outflow tract septation. Dev Biol. 2011;356(2):308-22.
1188 70. Henderson DJ, Conway SJ, Copp AJ. Rib truncations and fusions in the Sp2H mouse
1189 reveal a role for Pax3 in specification of the ventro-lateral and posterior parts of the somite.
1190 Dev Biol. 1999;209(1):143-58.
1191 71. Dickman ED, Rogers R, Conway SJ. Abnormal skeletogenesis occurs coincident
1192 with increased apoptosis in the Splotch (Sp2H) mutant: putative roles for Pax3 and
1193 PDGFRalpha in rib patterning. Anat Rec. 1999;255(3):353-61.
1194 72. Koushik SV, Chen H, Wang J, Conway SJ. Generation of a conditional loxP allele of
1195 the Pax3 transcription factor that enables selective deletion of the homeodomain. Genesis.
1196 2002;32(2):114-7.
1197 73. Zhou HM, Conway SJ. Restricted Pax3 Deletion within the Neural Tube Results in
1198 Congenital Hydrocephalus. J Dev Biol. 2016;4(1).
1199 74. Le Mouellic H, Lallemand Y, Brulet P. Homeosis in the mouse induced by a null
1200 mutation in the Hox-3.1 gene. Cell. 1992;69(2):251-64.
1201 75. Juan AH, Ruddle FH. Enhancer timing of Hox gene expression: deletion of the
1202 endogenous Hoxc8 early enhancer. Development. 2003;130(20):4823-34.
1203 76. van den Akker E, Fromental-Ramain C, de Graaff W, Le Mouellic H, Brulet P,
1204 Chambon P, et al. Axial skeletal patterning in mice lacking all paralogous group 8 Hox genes.
1205 Development. 2001;128(10):1911-21.
1206 77. Horan GS, Wu K, Wolgemuth DJ, Behringer RR. Homeotic transformation of
1207 cervical vertebrae in Hoxa-4 mutant mice. Proc Natl Acad Sci U S A. 1994;91(26):12644-8.
1208 78. Jeannotte L, Lemieux M, Charron J, Poirier F, Robertson EJ. Specification of axial
1209 identity in the mouse: role of the Hoxa-5 (Hox1.3) gene. Genes Dev. 1993;7(11):2085-96.
1210 79. Condie BG, Capecchi MR. Mice homozygous for a targeted disruption of Hoxd-3
1211 (Hox-4.1) exhibit anterior transformations of the first and second cervical vertebrae, the atlas
1212 and the axis. Development. 1993;119(3):579-95.
1213 80. Fromental-Ramain C, Warot X, Lakkaraju S, Favier B, Haack H, Birling C, et al.
1214 Specific and redundant functions of the paralogous Hoxa-9 and Hoxd-9 genes in forelimb and
1215 axial skeleton patterning. Development. 1996;122(2):461-72.
1216 81. Chen F, Capecchi MR. Targeted mutations in hoxa-9 and hoxb-9 reveal synergistic
1217 interactions. Dev Biol. 1997;181(2):186-96.
1218 82. Kondrashov N, Pusic A, Stumpf CR, Shimizu K, Hsieh AC, Ishijima J, et al.
1219 Ribosome-mediated specificity in Hox mRNA translation and vertebrate tissue patterning.
1220 Cell. 2011;145(3):383-97.
1221 83. Lee CC, Shih YC, Kang ML, Chang YC, Chuang LM, Devaraj R, et al. Naa10p
1222 Inhibits Beige Adipocyte-Mediated Thermogenesis through N-alpha-acetylation of
1223 Pgc1alpha. Mol Cell. 2019;76(3):500-15 e8.
1224 84. Qiu P, Shandilya H, D'Alessio JM, O'Connor K, Durocher J, Gerard GF. Mutation
1225 detection using Surveyor nuclease. Biotechniques. 2004;36(4):702-7.
1226 85. Dehairs J, Talebi A, Cherifi Y, Swinnen JV. CRISP-ID: decoding CRISPR mediated
1227 indels by Sanger sequencing. Sci Rep. 2016;6:28973.
1228 86. Wisniewski JR, Zougman A, Nagaraj N, Mann M. Universal sample preparation

1229 method for proteome analysis. Nat Methods. 2009;6(5):359-62.
1230 87. Rappsilber J, Mann M, Ishihama Y. Protocol for micro-purification, enrichment, pre-
1231 fractionation and storage of peptides for proteomics using StageTips. Nat Protoc.
1232 2007;2(8):1896-906.
1233 88. Cox J, Mann M. MaxQuant enables high peptide identification rates, individualized
1234 p.p.b.-range mass accuracies and proteome-wide protein quantification. Nat Biotechnol.
1235 2008;26(12):1367-72.
1236 89. Zeger SL, Liang KY. Longitudinal data analysis for discrete and continuous
1237 outcomes. Biometrics. 1986;42(1):121-30.

1238

1239

Supporting information

S1 Table. Genotypes of offspring from *Naa10*$^{+/-}$ female mice crossed to the *Naa10*$^{+/Y}$ male mice.

Genotype (Expected Mendelian %)	Naa10$^{+/Y}$ or Naa10$^{+/+}$ (50%)	Naa10$^{+/-}$ (25%)	Naa10$^{-/Y}$ (25%)
E10.5 (n=134)	62 (46.3%)	39 (29.1%)	33 (24.6%)
E13.5 (n=98)	53 (54.1%)	22 (22.4%)	23 (23.4%)
E18.5 (n=170)	82 (48.2%)	49 (28.8%)	39 (23.0%)
Adults (n=733)	438 (59.8%)	207 (28.2%)	88 (12.0%)

Expected and observed Mendelian ratio of genotypes in offspring at E10.5, E13.5, E18.5 and adults from crosses of *Naa10*$^{+/-}$ female and *Naa10*$^{+/Y}$ male mice. The percentage of adult *Naa10*$^{-/Y}$ mice significantly decreases.

S2 Table. Genotypes of offspring from *Naa10*$^{+/tm1a}$ female mice crossed to the *Naa10*$^{+/Y}$ male mice.

Genotype (Expected Mendelian %)	Naa10$^{+/Y}$ or Naa10$^{+/+}$ (50%)	Naa10$^{+/tm1a}$ (25%)	Naa10$^{tm1a/Y}$ (25%)
E10.5 (n=109)	55 (50.46%)	26 (23.85%)	28 (25.69%)
E12.5 (n=45)	20 (44.4%)	12 (26.7%)	13 (28.9%)
E18.5 (n=53)	27 (51.0%)	13 (24.5%)	13 (24.5%)
Adults (n=260)	152 (58.5%)	85 (32.7%)	23 (08.8%)

Expected and observed Mendelian ratio of genotypes in offspring at E10.5, E13.5, E18.5 and adults from crosses of *Naa10*$^{+/tm1a}$ female and *Naa10*$^{+/Y}$ male mice. The percentage of adults *Naa10*$^{tm1a/Y}$ mice significantly decreases.

S3 Table. Cervical fusion skeletal analyses in *Naa10* KO mice.

genotype	sample size	one or more fusion events	two or more fusion events	consecutive fusion events	C1+2 fusion	C2+3 fusion	C3+4 fusion	C4+5 fusion	C5+6 fusion	C6+7 fusion	C7+ T1 fusion	T1+2 fusion
Naa10$^{+/Y}$	19	2/17 (12%)	1/17 (6%)	0/17 (0%)	2/17 (12%)	0/18 (0%)	0/18 (0%)	0/19 (0%)	0/19 (0%)	0/19 (0%)	1/19 (5%)	0/19 (0%)
Naa10$^{+/+}$	4	1/4 (25%)	0/4 (0%)	0/4 (0%)	1/4 (25%)	0/4 (0%)	0/4 (0%)	0/4 (0%)	0/4 (0%)	0/4 (0%)	0/4 (0%)	0/4 (0%)
Naa10$^{+/-}$	4	1/4 (25%)	0/4 (0%)	0/4 (0%)	1/4 (25%)	0/4 (0%)	0/4 (0%)	0/4 (0%)	0/4 (0%)	0/4 (0%)	0/4 (0%)	0/4 (0%)
Naa10$^{-/Y}$	9	9/10 (90%)	3/9 (33%)	1/9 (11%)	7/10 (70%)	2/9 (22%)	2/9 (22%)	1/9 (11%)	0/9 (0%)	0/9 (0%)	1/9 (11%)	0/9 (0%)
Naa10$^{-/-}$	1	1/1 (100%)	1/1 (100%)	1/1 (100%)	1/1 (100%)	1/1 (100%)	0/1 (0%)	0/1 (0%)	0/1 (0%)	0/1 (0%)	0/1 (0%)	0/1 (0%)

S4 Table. Matings and litter size analyses.

	Naa10 KO matings, all WT/WT for Naa12, all >99.6% C57BL/6J						Naa10 x Naa12 matings, mixed genetic background	
Genotypes of breeders (♀ x ♂)	***Naa10*$^{+/+}$ x *Naa10*$^{+/Y}$**	***Naa10*$^{+/+}$ x *Naa10*$^{-/Y}$**	***Naa10*$^{+/-}$ x *Naa10*$^{+/Y}$**	***Naa10*$^{+/-}$ x *Naa10*$^{-/Y}$**	***Naa10*$^{-/-}$ x *Naa10*$^{-/Y}$**	***Naa10*$^{-/-}$ x *Naa10*$^{+/Y}$**	**Naa10$^{+/-}$ Naa12$^{+/+}$ x Naa10$^{+/Y}$ Naa12$^{+/-}$**	**Naa10$^{+/-}$ Naa12$^{+/+}$ x Naa10$^{+/Y}$ Naa12$^{-/-}$**
#pups	**255**	**18**	**330**	**59**	**59**	**127**	**191**	**21**
#litters	**39**	**2**	**66**	**13**	**11**	**31**	**38**	**5**
#pups/ #litters, or litter size	**6.5**	**9.0**	**5.0**	**4.5**	**5.4**	**4.1**	**5.0**	**4.2**
SD of litter size	**3.2**	**0.0**	**2.2**	**2.5**	**2.5**	**2.1**	**2.2**	**2.5**
% Died in 1st three days of life	**5.1%**	**5.6%**	**15.8%**	**13.6%**	**42.4%**	**36.0%**	**18.8%**	**28.6%**
% of total that died by weaning ~4 weeks	**5.9%**	**11.1%**	**23.0%**	**32.2%**	**59.3%**	**44.0%**	**22.0%**	**33.3%**
Avg Length of Mating till 1st Litter:	**29**	**22**	**34**	**25**	**35**	**28**	**26**	**63**
Total number of unique mating males:	**7**	**1**	**12**	**5**	**6**	**7**	**13**	**4**
Total number of mating pairs set up:	**8**	**1**	**>16**	**14**	**10**	**11**	**22**	**7**
Total number of mating pairs with progeny	**7**	**1**	**N/A**	**7**	**4**	**11**	**21**	**5**
% females who became pregnant and gave birth at least once:	**87.5%**	**100.0%**	**N/A**	**50.0%**	**40.0%**	**100.0%**	**95.5%**	**71.4%**

1268 **S5 Table. Genotypes of offspring from *Naa12*$^{+/-}$ female mice crossed to the *Naa12*$^{+/-}$ male mice.**

Genotype (Expected Mendelian %)	Naa12$^{+/+}$ (25%)	Naa12$^{+/-}$ (50%)	Naa12$^{-/-}$ (25%)
Adults (n=117)	**26 (22%)**	**62 (53%)**	**29 (25%)**

1269 Expected and observed Mendelian ratio of genotypes in offspring from crosses of *Naa12*$^{+/-}$ female and
1270 *Naa12*$^{+/-}$ male mice.
1271
1272
1273 **S6 Table. Mice analyzed by weighing, according to genotype.**

Females						
			Naa12 status			
			WT/WT	WT/KO	KO/KO	Total
Naa10 status	Pure C57BL/6J background Naa10 mice	WT/WT	67	N/A	N/A	67
		WT/KO	125	N/A	N/A	125
		KO/KO	15	N/A	N/A	15
		Subtotal	207	N/A	N/A	207
	mixed genetic background Naa10 and Naa12 mice	WT/WT	32	82	10	124
		WT/KO	35	23	0	58
		KO/KO	0	0	0	0
		Subtotal	67	105	10	182
	Total		274	105	10	389

1274

Males						
			Naa12 status			
			WT/WT	WT/KO	KO/KO	Total
Naa10 status	Pure C57BL/6J background Naa10 mice	WT	97	N/A	N/A	97
		KO	70	N/A	N/A	70
		Subtotal	167	N/A	N/A	167
	mixed genetic background Naa10 and Naa12 mice	WT	44	63	11	118
		KO	14	0	0	14
		Subtotal	58	63	11	132
	Total		225	63	11	299

1275
1276
1277
1278
1279
1280
1281
1282

S7 Table. Effects of *Naa10* KO on growth rate of *Naa10* mice on pure genetic background.

	C57BL/6J inbred females (N = 207)															
	Effect of age and age^2				Effect of Naa10 KO				Effect of age and Naa10 KO				Effect of age, Naa10 KO, and interaction			
	Coeff.	SE	z	p > |z|	Coeff.	SE	z	p > |z|	Coeff.	SE	z	p > |z|	Coeff.	SE	z	p > |z|
Age in days	0.349	0.006	59.49	< 0.001					0.349	0.006	59.38	< 0.001	0.344	0.010	34.59	< 0.001
Age^2	- 0.001	0.00003	- 40.59	< 0.001					- 0.001	0.00003	- 40.56	< 0.001	- 0.001	0.00005	- 24.53	< 0.001
Naa10 KO					- 2.92	0.847	- 3.45	0.001	- 0.252	0.248	- 1.01	ns	- 0.219	0.451	- 0.49	ns
Age x KO													0.009	0.012	0.75	ns
Age^2 x KO													- 0.00009	0.00007	-1.27	ns
(constant)	2.518	0.204	12.35	< 0.001	17.23	0.690	24.96	< 0.001	2.697	0.272	9.93	< 0.001	2.633	0.382	6.90	< 0.001
Wald X^2 [a]	6547.29, p < 0.0001				11.93, p = 0.0006				6552.24, p < .0001				6611.63, p < 0.0001			

	C57BL/6J inbred males (N = 167)															
	Effect of age and age^2				Effect of Naa10 KO				Effect of age and Naa10 KO				Effect of age, Naa10 KO, and interaction			
	Coeff.	SE	z	p > |z|	Coeff.	SE	z	p > |z|	Coeff.	SE	z	p > |z|	Coeff.	SE	z	p > |z|
Age in days	0.454	0.008	60.16	< 0.001					0.454	0.007	62.20	< 0.001	0.467	0.009	51.68	< 0.001
Age^2	- 0.002	0.00005	- 39.76	< 0.001					-0.002	0.00004	- 41.16	< 0.001	- 0.002	0.00005	- 34.53	< 0.001
Naa10 KO					- 4.721	1.040	- 4.54	< 0.001	-2.578	0.304	- 8.47	< 0.001	- 1.351	0.504	- 2.68	0.007
Age x KO													- 0.035	0.015	- 2.32	0.020
Age^2 x KO													0.0001	0.00009	1.46	ns
(constant)	1.303	0.271	4.81	< 0.001	19.56	0.668	29.28	< 0.001	2.430	0.283	8.58	< 0.001	1.931	0.321	6.01	< 0.001
Wald X^2 [a]	7220.56, p < 0.0001				20.60, p < 0.0001				8007.09, p < 0.0001				8185.75, p < 0.0001			

[a] The Wald X^2 is a measure of the overall goodness of fit of the complete model.

S8 Table. Effects of *Naa10* and *Naa12* KOs on growth rate on mixed genetic background

	females (N = 182): effects of age and knockouts on weight																			
	Effect of age and age^2				Effects of age and Naa10 KO				Effects of age and Naa12 KO				Effects of age, Naa10 & Naa12 KOs				Effects: age, Naa10, Naa12, both KOs			
	Coeff	SE	z	p > |z|	Coeff	SE	z	p > |z|	Coeff	SE	z	p > |z|	Coeff	SE	z	p > |z|	Coeff	SE	z	p > |z|
Age	.	0.011	43.10	< 0.001	0.489	0.011	45.02	< 0.001	0.489	0.011	43.25	< 0.001	0.491	0.011	46.16	< 0.001	0.492	0.011	46.49	< 0.001
Age^2	-0.003	0.0001	-24.47	< 0.001	-0.003	0.0001	-25.58	< 0.001	-0.003	0.0001	-24.55	< 0.001	-0.003	0.0001	-26.21	< 0.001	-0.003	0.0001	-26.45	< 0.001
Naa10					-1.117	0.254	-4.40	< 0.001					-1.424	0.267	-5.33	< 0.001	-0.368	0.335	-1.10	ns
Naa12-Het									-0.377	0.247	-1.53	ns	-0.789	0.255	-3.09	0.002	0.039	0.287	0.14	ns
Naa12-Ho									-0.659	0.625	-1.05	ns	-1.376	0.621	-2.21	0.027				
Naa10-Naa12-Het																	-2.143	0.510	-4.20	< 0.001
(constant)	0.616	0.264	2.33	0.020	0.966	0.267	3.61	< 0.001	0.825	0.291	2.83	0.005	1.508	0.307	4.91	< 0.001	0.879	0.307	2.86	0.004
Wald X^2 [a]	4692.14, p < 0.0001				5116.03, p < 0.0001				4752.14, p < 0.0001				5396.11, p < 0.0001				5461.46, p < 0.0001			

	females (N = 182): effects of age and knockouts on growth rate															
	Effects of age, Naa10 KO, interaction with age				Effects of age, Naa12 KO, interaction with age				Effects of age, both KOs & interaction with age				Effects: age, KOs & interaction with ea. other			
	Coeff	SE	z	p > |z|	Coeff	SE	z	p > |z|	Coeff	SE	z	p > |z|	Coeff	SE	z	p > |z|
Age	0.508	0.013	39.24	< 0.001	0.491	0.015	32.64	< 0.001	0.523	0.018	29.09	< 0.001	0.496	0.011	46.35	< 0.001
Age^2	-0.003	0.0001	-22.76	< 0.001	-0.003	0.0002	-17.97	< 0.001	-0.003	0.0002	-16.71	< 0.001	-0.003	0.0001	-26.24	< 0.001
Naa10	0.109	0.547	0.20	ns					0.030	0.582	0.05	ns	-0.364	0.336	-1.08	ns
Age x Naa10	-0.059	0.023	-2.51	0.012					-0.068	0.025	-2.76	0.006				
Age^2 x Naa10	0.0006	0.0002	2.25	0.024					0.0006	0.0003	2.46	0.014				
Naa12-Het					-0.175	0.547	-0.32	ns	-0.099	0.557	-0.18	ns	0.036	0.288	0.13	ns
Age x Naa12-Het					-0.005	0.023	-0.23	ns	-0.029	0.023	-1.23	ns				
Age^2 x Naa12-Het					0.000004	0.0002	0.02	ns	0.0002	0.0002	0.97	ns				
Naa12-Ho					-0.882	1.584	-0.56	ns	-0.916	1.551	-0.59	ns				
Age x Naa12-Ho					0.003	0.073	0.04	ns	-0.029	0.071	-0.41	ns				
Age^2 x Naa12-Ho					0.00003	0.0007	0.04	ns	0.0003	0.001	0.47	ns				
Naa10-Naa12-Het													0.784	1.303	0.60	ns
Age x Naa10-Naa12-Het													-0.113	0.052	-2.15	0.031
Age^2 x Naa10-Naa12-Het													0.0009	0.0005	1.73	ns
(constant)	0.588	0.305	1.93	ns	0.756	0.348	2.17	0.030	0.790	0.426	1.85	ns	0.774	0.309	2.50	0.012
Wald X^2 [a]	5224.04, p < 0.0001				4758.89, p < 0.0001				5526.71, p < 0.0001				5586.86, p < 0.0001			

Het : heterozygous
Ho : homozygous

[a] The Wald X^2 is a measure of the overall goodness of fit of the complete model.

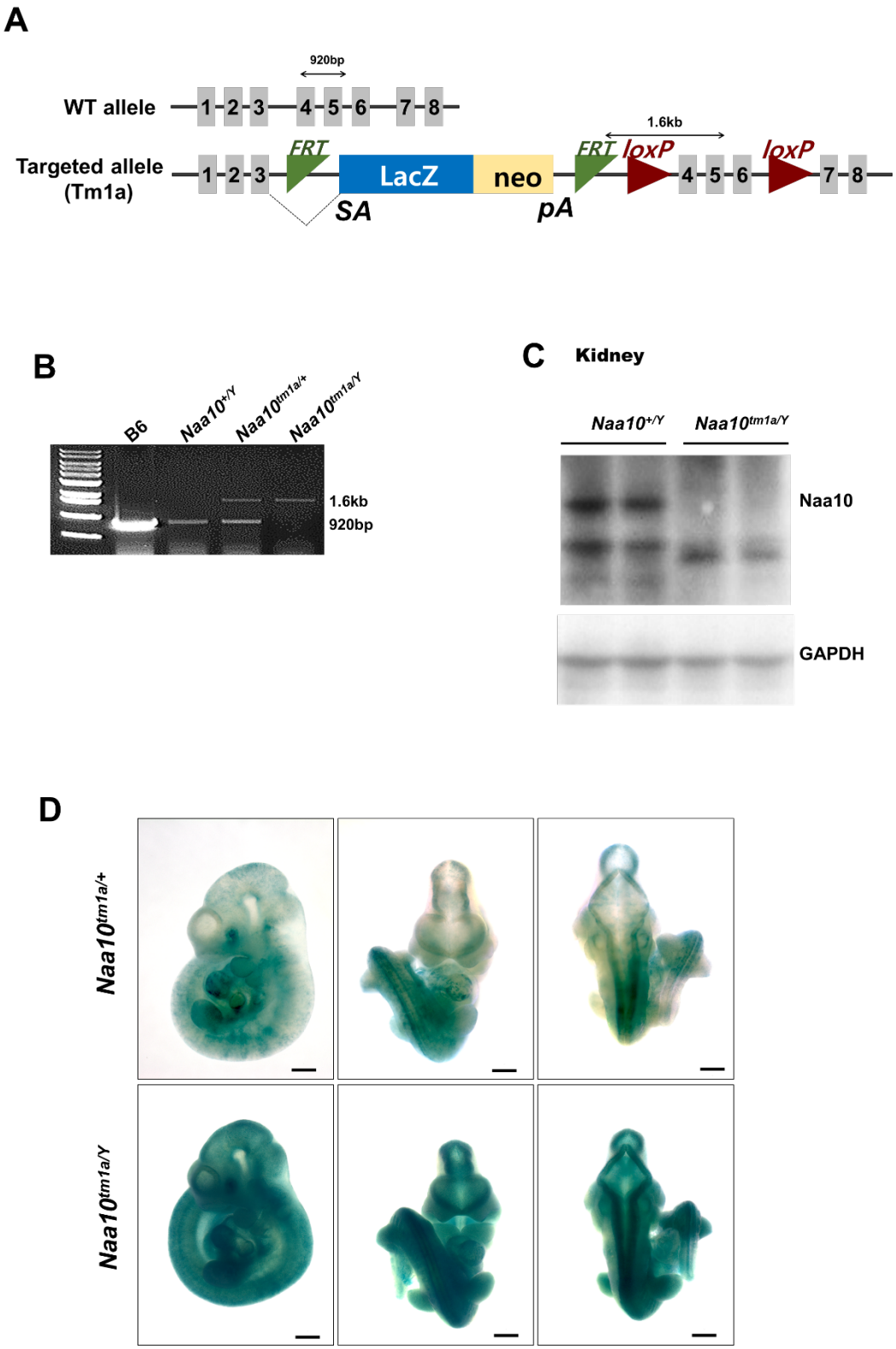

S1 Fig. Generation and confirmation of Naa10tm1a mice. (A) Schematic illustration of the Naa10tm1a mice. (B) PCR confirmation of Naa10 deficiency. (C) Confirmation of Naa10 protein in kidney tissue by Western blot. Naa10 protein is not detected in *Naa10*$^{-/Y}$ mouse. (D) Expression pattern of Naa10 in the embryo. β-gal staining represent Naa10 localization.

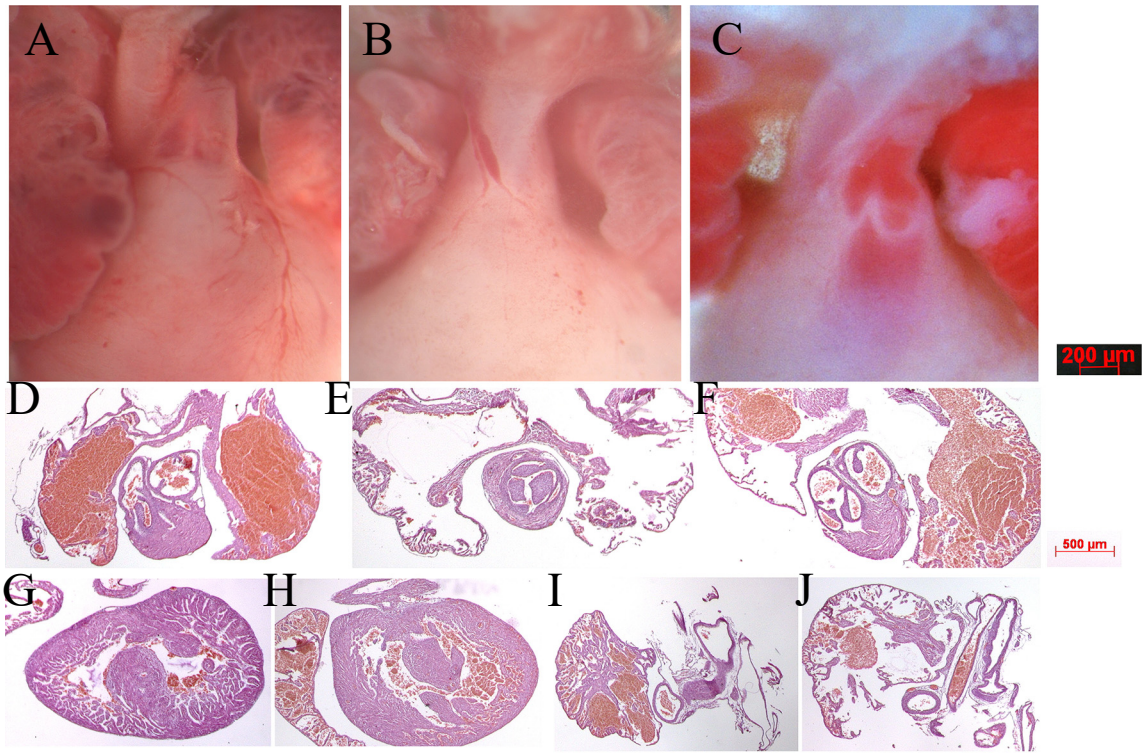

S2 Fig. Gross anatomy and histology of neonatal mouse hearts. (A) Wildtype male heart outflow tract region indicating separate aorta and pulmonary trunks nestled between left and right atria. (B) Naa10$^{-/-}$ female heart from dying P0 pup only has a single outflow tract emerging from the right ventricle, resulting in persistent truncus arteriosus. (C) Naa10$^{-/y}$ male heart from dying P0 pup has separate outflow tracts but both emerge from the right ventricle, resulting in double outlet right ventricle. (D) normal histology from wildtype male heart of pulmonary artery exiting the right ventricle. (E) histology from Naa10$^{-/-}$ heart of single outflow tract exiting the right ventricle with tricuspid valve leaflets. (F) histology from Naa10$^{-/y}$ heart of both pulmonary and aortic arteries emerging from right ventricle within the same plane. (G) Naa10$^{-/-}$ histology showing membranous VSD, (H) Naa10$^{-/y}$ histology showing muscular VSD. (I) normal heart revealing closed ductus arterious, J) Naa10$^{-/-}$ histology showing open ductus arterious leading to pulmonary overload and likely lethality.

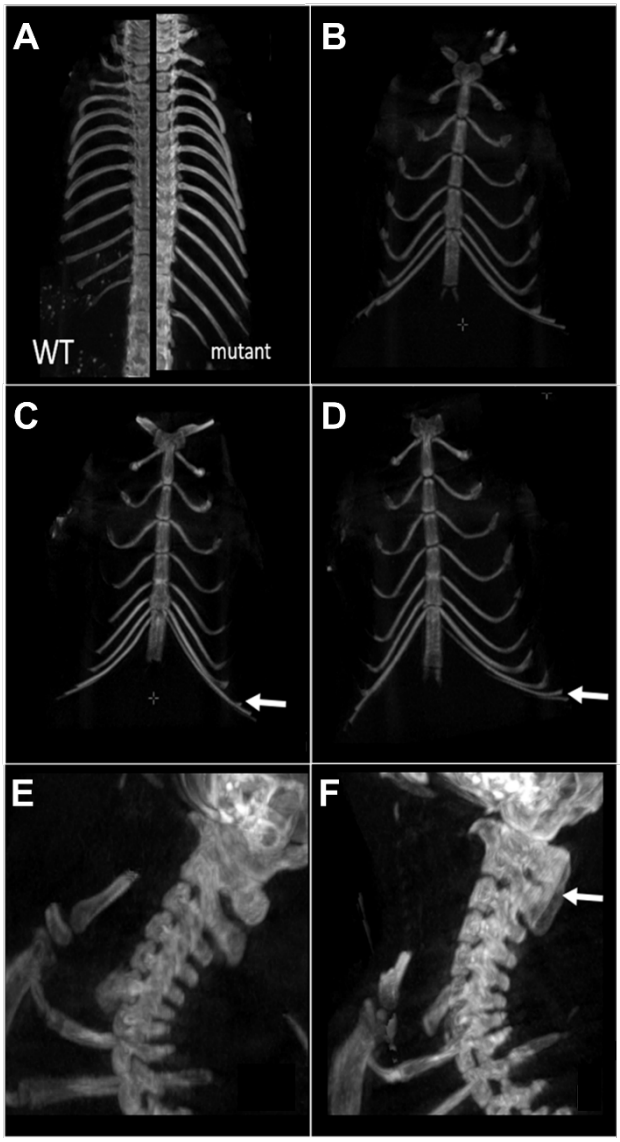

S3 Fig. Skeletal phenotype by CT scanning. (A) In WT mice 13 thoracic vertebrae and ribs are numbered whereas 14 thoracic vertebrae and ribs are counted in mutants (*Naa10*$^{-/Y}$) (WT on the left, mutant on the right). n=11 CT scans for *Naa10*$^{-/Y}$ compared to n=18 *Naa10*$^{+/Y}$. (B-D) Different number of ribs are linking the sternum between in *Naa10*$^{-/Y}$, *Naa10*$^{-/-}$ and WT. (B) 7 ribs linking the sternum in WT. (C) 8 ribs linking the sternum (the white arrow shows the 8th rib) in Naa10$^{-/Y}$. (D) 7 on one side + 7 and one almost linking on the other side. In 2 mice, an asymmetrical link was observed. White arrow shows the eighth asymmetrical rib. (E and F) Abnormalities in the cervical phenotype. (E) Cervical WT/ morphology. (F) Partial fusion of C1 and C2 dorsal arch in one mutant mouse.

1356

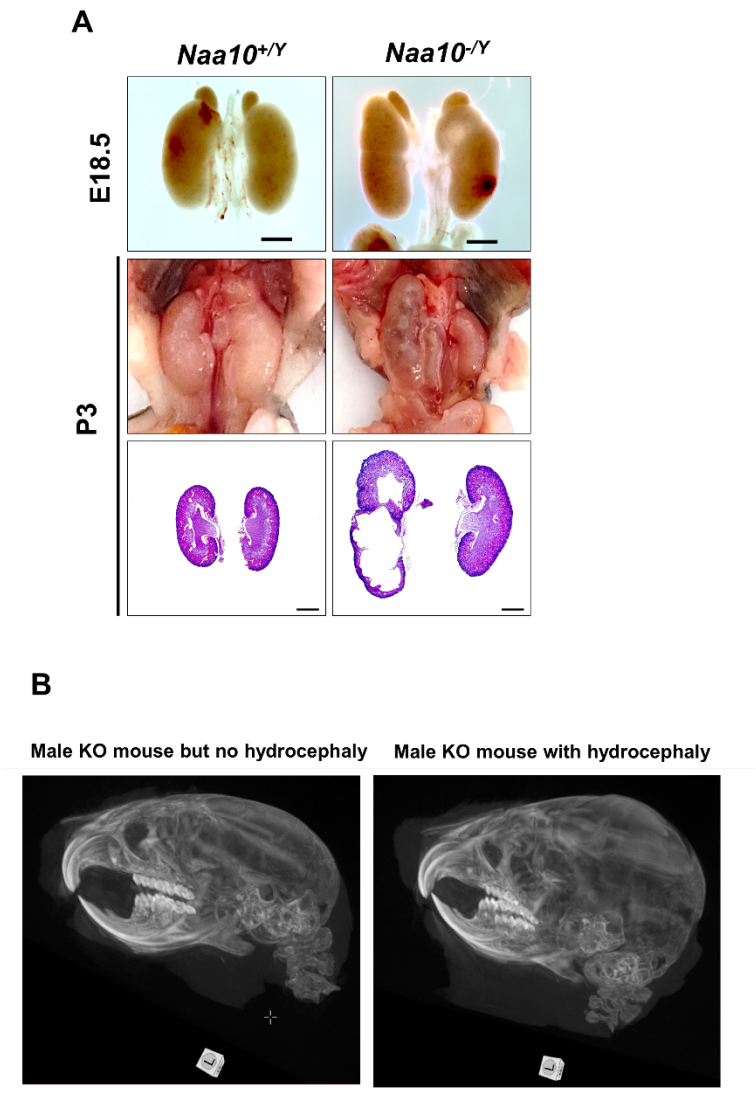

1357

1358 **S4 Fig. Hydronephrosis and Hydrocephaly in Naa10 KO mice.** (A) Representative images
1359 and histology of renal defects at E18.5 (n=6 out of 39 examined) and P3 (n= 4 out of 11
1360 examined). (B) Hydrocephaly (n=3 CT scans for *Naa10*$^{-/Y}$ mice with hydrocephaly compared
1361 to n=3 *Naa10*$^{-/Y}$ mice without hydrocephaly).

1362

1363

1364

1365

1366

1367

1368

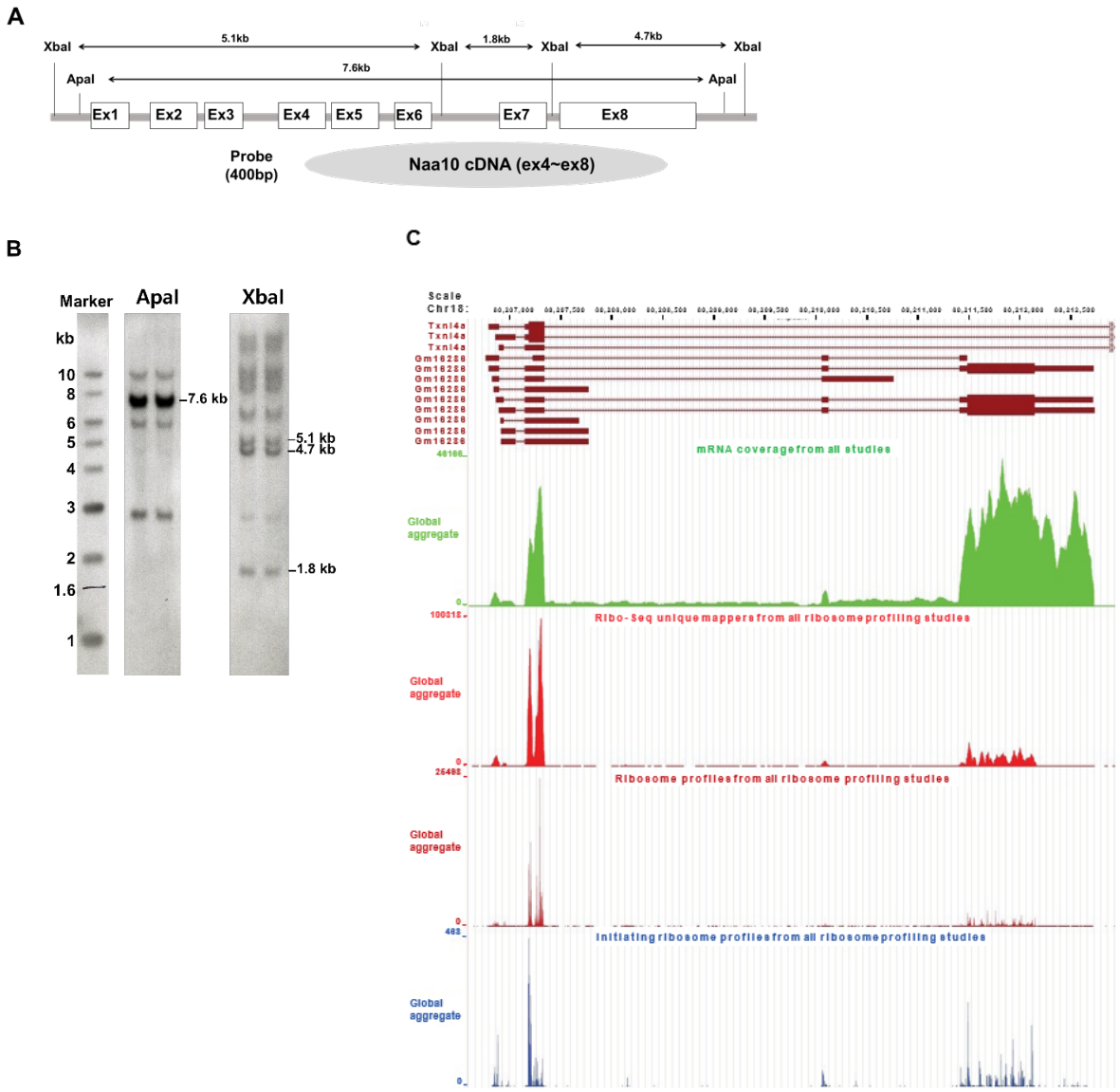

S5 Fig. Identification of a potential Naa10 homolog. (A) Construction of *Naa10* Southern blot probe. (B) Southern blot membrane after hybridization with a *Naa10* probe. Expected size band, restricted with Apa I and Xba I, were showed. (C) Ribosome profiling traces for the potential *Naa10* paralog (Gm16286, UniProt: Q9CQX6). Picture was modified from GWIPS genome browser, Chr 18, 80206601-80212942.

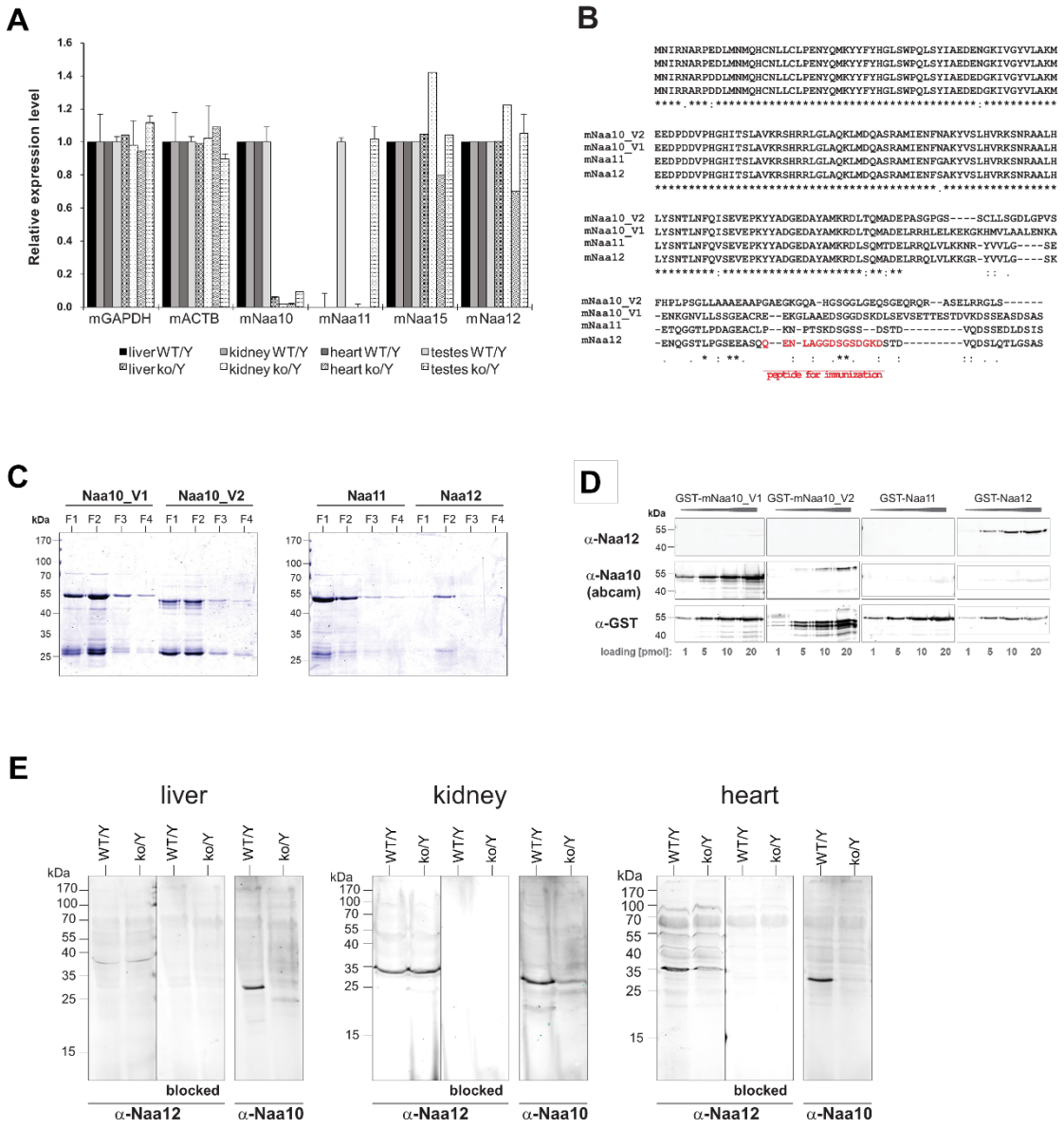

S6 Fig. Characterization of a potential Naa10 homolog. (A) qPCR analyses of mouse NATs (mNATs) in *Naa10* WT and KO mouse tissue. (B) Sequence alignment of mNaa10 isoforms and paralogs, including the potential Naa10 paralog mNaa12 (Gm16286, UniProt: Q9CQX6) using Clustal Omega (EMBL-EBI). The peptide used for immunization of rabbits to generate a specific antibody is indicated in red. (C) Full length mNAT cDNA from mouse was amplified and cloned into pGEX-4T1. Proteins were expressed in E. coli BL21 (DE3) and purified via GSH-sepharose. Shown is a coomassie stain of fraction 1-4. (D) Cross-reactivity and sensitivity of the used NAT antibodies. 1-20 pmol of GST-mNAT proteins were separated on SDS-PAGE followed by western blot, probed with the indicated antibodies. (E) Detection of endogenous mNaa12. Tissue lysate from liver, kidney and heart were subjected to SDS-PAGE and WB. Right panel of Naa12 shows antibody competition assay.

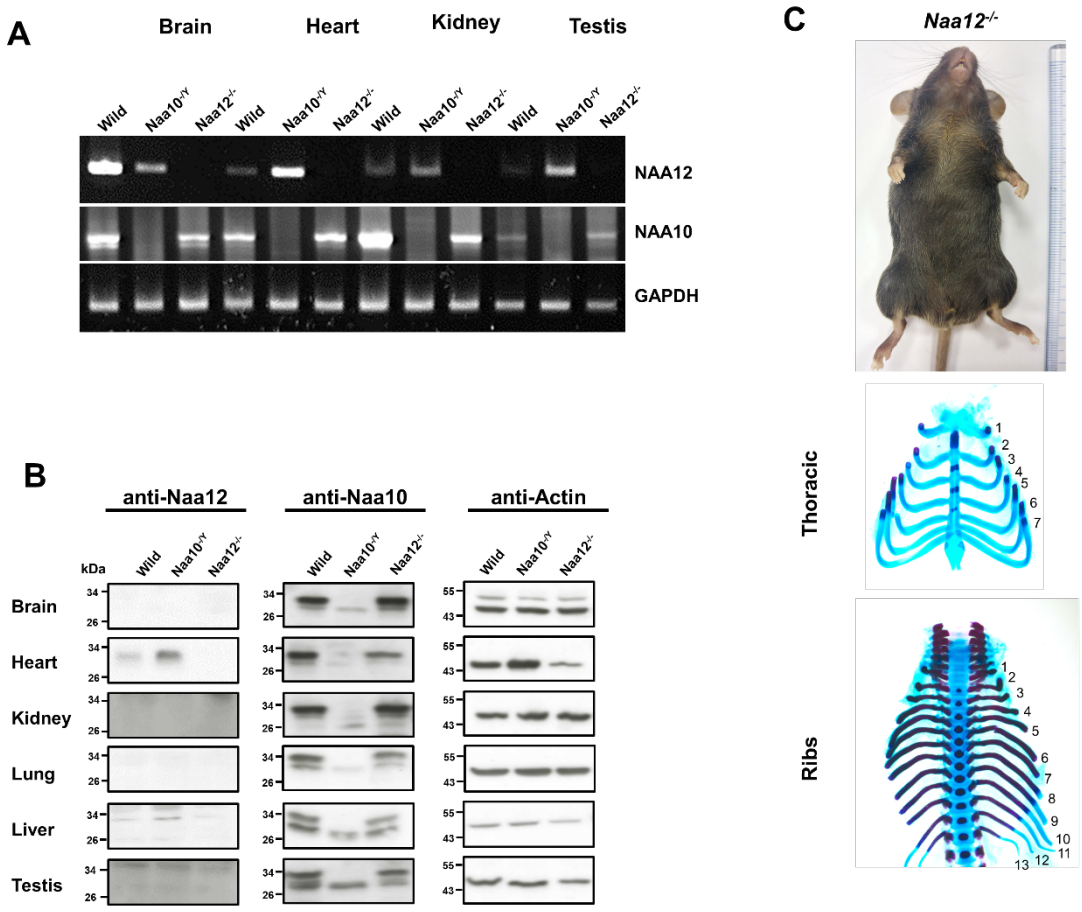

S7 Fig. Confirmation and characterization of Naa12 KO mice. (A) Expression of *Naa10* and *Naa12* in WT, *Naa10* KO and *Naa12* KO tissues (brain, heart, kidney and testis) by RT-PCR. Expression of GAPDH was analyzed as an endogenous control. (B) Expression of Naa12 protein determined in WT, *Naa10* KO and *Naa12* KO tissues (brain, heart, kidney, lung, liver and testis) by Western blot analysis. (C) Phenotypes in *Naa12* KO mice. Lack of hypopigmentation (upper; N=29) and lack of supernumerary ribs (middle and bottom; E18.5; N=7) in *Naa12* KO mouse.

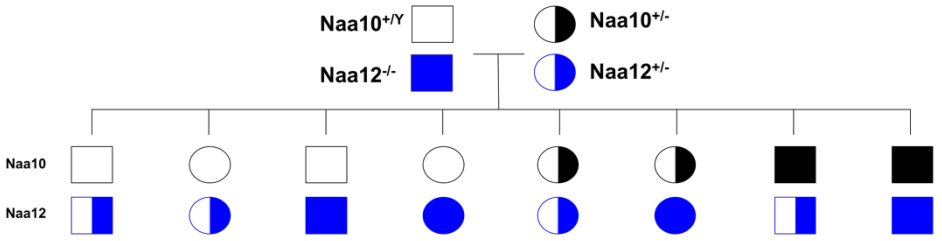

Genotype	Naa10$^{+/Y}$ Naa12$^{+/-}$	Naa10$^{+/+}$ Naa12$^{+/-}$	Naa10$^{+/Y}$ Naa12$^{-/-}$	Naa10$^{+/+}$ Naa12$^{-/-}$	Naa10$^{+/-}$ Naa12$^{+/-}$	Naa10$^{+/-}$ Naa12$^{-/-}$	Naa10$^{-/Y}$ Naa12$^{+/-}$	Naa10$^{-/Y}$ Naa12$^{-/-}$	Unable to genotype
E8.5 (n=21)	1	4	7	6	2	1	0	0	4
E10.5 (n=28)	3	3	4	8	8	1*	1*	0	12
E12.5 (n=25)	7	4	6	1	7	0	0	0	19
E18.5 (n=11)	0	2	4	2	3	0	0	0	7
Postnatal (n=179)	40	45	47	35	12	0	0	0	2

* lysed embryo

S8 Fig. Genotypes of offspring from *Naa10*$^{+/-}$; *Naa12*$^{+/-}$ female mice crossed to the *Naa10*$^{+/Y}$; *Naa12*$^{-/-}$ male mice. *Naa10*; *Naa12* DKO exhibit embryonic lethality. Pedigree of mating and genotypes of pups and embryos at E8.5, E10.5, E12.5 and E18.5.